Environmental Science and Pollution Research (2023) 30:45528–45554
https://doi.org/10.1007/s11356-023-25822-y

REVIEW ARTICLE

Current trends in carbon-based quantum dots development from solid wastes and their applications

Chanchal Das[1] · Mika Sillanpää[2] · Shabi Abbas Zaidi[3] · Moonis Ali Khan[4] · Goutam Biswas[1]

Received: 13 November 2022 / Accepted: 5 February 2023 / Published online: 21 February 2023

Abstract

Urbanization and a massive population boom have immensely increased the solid wastes (SWs) generation and are expected to reach 3.40 billion tons by 2050. In many developed and emerging nations, SWs are prevalent in both major and small cities. As a result, in the current context, the reusability of SWs through various applications has taken on added importance. Carbon-based quantum dots (Cb-QDs) and their many variants are synthesized from SWs in a straightforward and practical method. Cb-QDs are a new type of semiconductor that has attracted the interest of researchers due to their wide range of applications, which include everything from energy storage, chemical sensing, to drug delivery. This review is primarily focused on the conversion of SWs into useful materials, which is an essential aspect of waste management for pollution reduction. In this context, the goal of the current review is to investigate the sustainable synthesis routes of carbon quantum dots (CQDs), graphene quantum dots (GQDs), and graphene oxide quantum dots (GOQDs) from various types SWs. The applications of CQDs, GQDs, and GOQDs in the different areas are also been discussed. Finally, the challenges in implementing the existing synthesis methods and future research directions are highlighted.

Keywords Solid wastes · Carbon-based quantum dots · Carbon quantum dots · Graphene quantum dots · Graphene oxide quantum dots

Abbreviations

1D-NMR	One-dimensional nuclear magnetic resonance
2D-NMR	Two-dimensional nuclear magnetic resonance
AFM	Atomic force microscope
BET	Brunauer-Emmett-Teller
Cb-QDs	Carbon-based quantum dots
CFU	Colony-forming unit
CNTs	Carbon nanotubes
-COOH	Carboxyl group
CP-MAS-^{13}C-NMR	Solid state cross polarization/magnetic angle spinning ^{13}C nuclear magnetic resonance spectroscopy
CQDs	Carbon quantum dots
DLS	Dynamic light scattering
DNA	Deoxyribonucleic acid
EDX	Energy dispersive X-ray
EPA	Environmental protection agency
FTIR	Fourier transform infrared
GO	Graphene oxide
GOQDs	Graphene oxide quantum dots
GQDs	Graphene quantum dots
GSH	Glutathione
GSH@rCQDs	Glutathione modified reduced carbon quantum dots
HOMO	Highest occupied molecular orbital
HRTEM	High-resolution transmission electron microscopy
HSQC	Heteronuclear single quantum coherence

Responsible Editor: George Z. Kyzas

✉ Moonis Ali Khan
mokhan@ksu.edu.sa

[1] Department of Chemistry, Cooch Behar Panchanan Barma University, West Bengal, Cooch Behar 736101, India

[2] Department of Chemical Engineering, School of Mining, Metallurgy and Chemical Engineering, University of Johannesburg, P. O. Box 17011, Doornfontein 2028, South Africa

[3] Department of Chemistry and Earth Sciences, College of Arts and Sciences, Qatar University, 2713 Doha, Qatar

[4] Department of Chemistry, College of Science, King Saud University, Riyadh 11451, Saudi Arabia

LGQDs	Lignin-based graphene quantum dots
LPEI	Linear-polyethyleneimine
LUMO	Lowest unoccupied molecular orbital
N@CQDs	Nitrogen-doped carbon quantum dots
N@mCQDs	Nitrogen-doped microporous carbon quantum dots
$NaBH_4$	Sodium borohydride
$-NH_2$	Amino
-OH	Hydroxyl group
PEI	Branched polyethyleneimine
PA	Picric acid
PL	Photoluminescence
ppb	Parts per billion
PXRD	Powder X-ray diffractometry
QD	Quantum dot
QDs	Quantum dots
QY	Quantum yield
rCQDs	Reduced carbon quantum dots
ROS	Reactive oxygen species
RS	Raman spectroscopy
S@GQDs	Sulphur-doped graphene uantum dots
SAED	Selected area electron diffraction
SEM	Scanning electron microscopy
$-SO_2-$	Sulfur-containing groups
$-SO_3H$	Sulphonic acid group
w/w	Weight/weight ratio
SW-materials	Solid waste-materials
SWs	Solid wastes
TCSPC	Fluorocube time-correlated single photon counting
TCSPC	Time correlated photon counting
TGA	Thermogravimetric analysis
TRPL	Time resolved photoluminescence
UV-Vis	UV-visible absorption
XPS	X-ray photoelectron spectroscopy

Introduction

The generation of solid wastes (SWs) has increased dramatically as a result of urbanization and significant population growth and is anticipated to reach 3.40 billion tons by 2050 ("Solid Waste Management" n.d.). Thus, SWs treatment and disposal is a critical issue that must be addressed by both developing and developed countries, particularly in metropolitan areas (Bui et al. 2022; Khan et al. 2021). Generally, these SWs are a collection of agricultural, paper, food, animal, yard trimming, plastics, metals, rubber, leather, textiles, wood, glass wastes, and so on (Fig. 1) (Abdel-Shafy and Mansour 2018). The continuous rise in ecologically harmful and hazardous SWs is currently a major concern, necessitating either proper trash disposal or reuse (Meyer et al. 2020). According to reports, over 70% of the global SWs are disposed of in landfills, while only 20% are recycled. As a result, it is imperative to enhance the proportion of SWs recycled into valuable goods.

Because of the high cost, lack of organization, and difficulties, sustainable management of these SWs is the

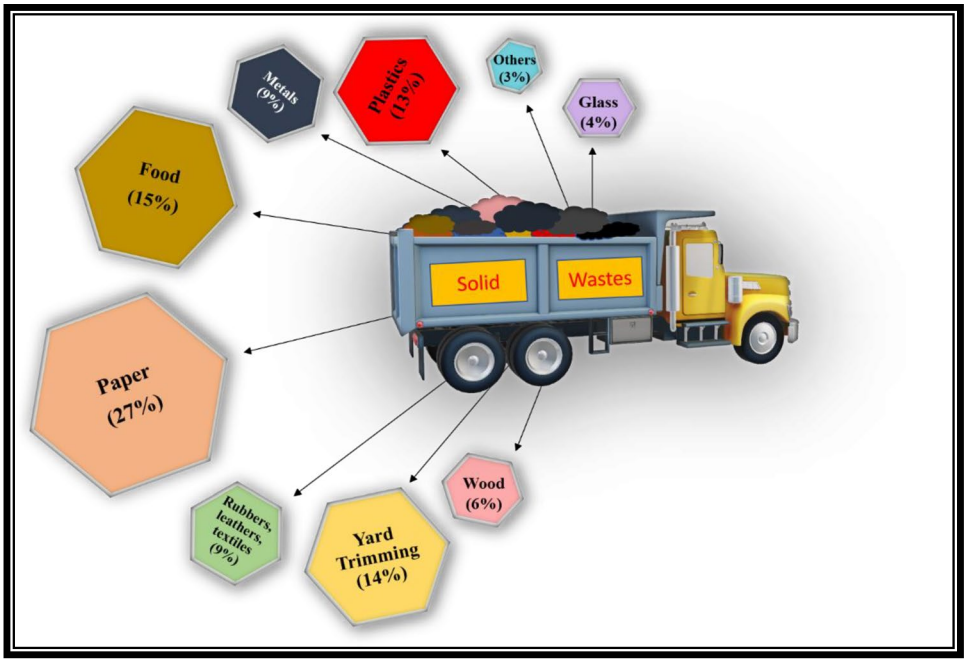

Fig. 1 Globally available common solid waste materials

most significant impediment to increasing urbanization and an improvement in the standard of living (Chien et al. 2021; Khan et al. 2022). Thus, the proposed management method must be cost-effective, simple, sustainable, and ecologically appealing, as well as legally and socially permissible. Because most agricultural, household, human, and animal wastes are rich in proteins, minerals, and carbohydrates, thus, these SWs can be used as raw materials in material science and other related areas.

Owing to their wide range of applications in physical, chemical, biological, and materials research, nanomaterials are a revolutionary finding of the late twentieth century (Das et al. 2020; 2022; Kolahalam et al. 2019; Sasidharan et al. 2019; Talapin and Shevchenko 2016; Rajabi et al. 2020, 2018; Wei et al. 2017; Zang et al. 2017; Liu et al. 2018; Vatanpour et al. 2022; Fakhraie et al. 2023). Generally, they have different physicochemical properties compared to their bulk counterparts. Quantum dots (QDs) are a subset of nanomaterials that were envisioned in the 1980s, when charge transporters were confined to three-dimensional semiconductor materials (Das et al. 2018; Lv et al. 2020). Carbon onions (Dalal et al. 2021; Lettieri et al. 2017a, b), carbon nanotubes (Gao et al. 2014; Li and Shi 2014; Spreinat et al. 2021; Welsher et al. 2009), carbon nanoribbons (Lu et al. 2009; Wang et al. 2019a; Zhao et al. 2017), CQDs (Hu et al. 2014a; Khan et al. 2017; Wang et al. 2016a, 2021), GQDs (Facure et al. 2020; Tabish and Zhang 2016), GOQDs (Cunci et al. 2021; Tang et al. 2016), and other types of Cb-QDs (Liu et al. 2020; Tao et al. 2019) have been evolved as distinct forms of Cb-QDs based on their size, shape, and structural variations (Liu et al. 2020; Tajik et al. 2020).

The first type of CQDs was serendipitously synthesized in 2004 (Xu et al. 2004) as a spherically symmetrical materials between the amorphous and crystalline states with < 10 nm size. The QDs are appealing to researchers due to their biocompatibility, low toxicity, high solubility, high water stability, ease of functioning, catalytic activity, and variable fluorescence (Rasal et al. 2021; Wareing et al. 2021) properties. QDs, due to their unique properties, can be used for a variety of applications, including biomedical (Alaghmandfard et al. 2021; Chen et al. 2017; Chiu et al. 2016; Nair et al. 2020), wastewater treatment (Kusic et al. 2011; Rani et al. 2020), catalysis (Chen et al. 2020; Huang et al. 2018; Reshak 2017; Tian et al. 2021; Yang et al. 2014; Zammataro and Sfrazzetto 2019), energy storage (Kumar et al. 2020a; Rasal et al. 2021), and metal ion sensing (Algar et al. 2021; Li et al. 2019; Rosso et al. 2020). This review focuses on carbon-enriched SWs such as fruit peels, shells, and waste toner as a source of carbon-based fluorescent materials, i.e. Cb-QDs. In this work, the articles reporting waste conversion to carbon/graphene/graphene oxide quantum dots were comprehensively summarized.

The respective Cb-QDs can be synthesized using one of the two major approaches: top-down or bottom-up (Bruno et al. 2021; Muñoz et al. 2021; Valizadeh et al. 2012). The top-down approach employed macroscopic materials such as coal, graphene, and diverse natural products from various plant parts including leaves, fruits, and stems etc. (Alvand et al. 2021; Moradi Alvand et al. 2019b, 2019a; Rajabi et al. 2020) which are decomposed to produce the appropriate Cb-QDs. In contrast, in the bottom-up technique, various types of carbonaceous smaller molecules taken as precursors are chemically modified under suitable reaction conditions to obtain fluorescent Cb-QDs (Xu et al. 2020). Both the top-down and bottom-up approach possess some advantages and few disadvantages, e.g., in general bottom-up methods are cost-effective compared to the top-down; large scale production is easy in top-down approach while this becomes difficult in bottom-up method; in bottom-up approach impurity remains, hence need to purify, whereas in top-down, chemical purification is rarely required. In top-down method, size distribution is broader compared to bottom-up approach (Al Jahdaly et al. 2021; Desmond et al. 2021).

Most of the previous review articles have focused on the synthesis, characterization, and application of Cb-QDs. To date, only few reviews appeared on SWs-derived CQDs, GQDs, and GOQDs, suggesting further research and development in this critical field (Arias Velasco et al. 2021; Nasrollahzadeh et al. 2021; Tatrari et al. 2021). This review, for the first time, has summarized the three types of SWs-derived QDs based on synthesis, characterization, and applications. Previously, Rani et al. (2020) briefly reviewed the features of these QDs based on various characterization techniques. However, this review article analyzes practical applications and future potentials of Cb-QDs by critically reviewing publications on SWs-derived Cb-QDs. Current work is also intended to describe the synthesis and characterization of Cb-QDs with potential issues. This article will give future researchers an elaborate idea of what was investigated and what remained in waste-derived Cb-QDs.

Synthesis methodology

As stated previously, Cb-QDs can be synthesized using either top-down or bottom-up techniques, depending on their high crystallinity, monodispersity, and homogeneity. Bottom-up approaches include hydrothermal carbonization (Gomes et al. 2019), chemical oxidation (Liu et al. 2016), micro-fluidization (Buzaglo et al. 2016), microwave-assisted methods (Rodríguez-Padrón et al. 2018), and electrochemical methods (Ahirwar et al. 2017), whereas the common and most applied top-down approaches are ball milling (Youh et al. 2020), ultrasonication (Kumar et al. 2020b), hydrothermal (Wu et al. 2017), liquid exfoliation, pyrolysis (Zdrazil

et al. 2018), and electron beam lithography (Tian et al. 2018). Most of the methods utilized economically appealing reaction conditions and SWs as precursor materials, ranging from field to industry. These techniques can produce Cb-QDs with or without fabrication. Fabrication effectively prevents QDs from aggregating into larger counterpart and may adjust various types of physicochemical qualities, allowing the QDs to be used in desired directions. The conversion yields for these SWs into the corresponding luminous materials are very poor; therefore, they are avoided and replaced with quantum yields (QYs). The following subsections will deal in various synthesis methodologies of transforming SWs to CQDs.

Synthesis of carbon quantum dots

CQDs are synthesized from a variety of biodegradable sources, such as manure (D'Angelis do E. S. Barbosa et al. 2015; Horst et al. 2021), hair (Guo et al. 2016; Liu et al. 2014; Singh et al. 2020), plant roots (D'souza et al. 2018; Yu et al. 2019), stems (Vandarkuzhali et al. 2017), fruit and vegetable peels and shells (Ang et al. 2020; Atchudan et al. 2021; Bankoti et al. 2017; Cheng et al. 2017; Hu et al. 2021; Prasannan and Imae 2013; Qureshi et al. 2021; Rajamanikandan et al. 2021; Surendran et al. 2020; Tyagi et al. 2016; Vandarkuzhali et al. 2018; Wang et al. 2020; Xue et al. 2016; Yang et al. 2021), tea waste (Chen et al. 2019; Zhu et al. 2019), wheat straw (S. Liu et al. 2021a, b; Yuan et al. 2015), animal shell (Gedda et al. 2016; Yao et al. 2017), expired milk (Athika et al. 2019; Su et al. 2018), feathers (Liu et al. 2015; Ye et al. 2017), egg shell (Pramanik et al. 2018; Wang et al. 2012; Ye et al. 2020), whey (Devi et al. 2017), waste paper (Devi et al. 2018; Jeong et al. 2018; Park et al. 2020), cat feedstocks (Ahn et al. 2019), soot (Thulasi et al. 2020; Tripathi et al. 2014; Venkatesan et al. 2019), waste oil (Y. Hu et al. 2014a, b; Mahat and Shamsudin 2020), petroleum coke (Wang et al. 2015a), sugarcane waste (Pandiyan et al. 2020; Xu-Cheng et al. 2018), rice waste (Anthony et al. 2020; Nguyen et al. 2021), and waste pulp (D et al. 2019).

CQDs of 2.5 nm were prepared by Vandarkuzhali et al. (2017) from ethanolic extract of the pseudo-stem of banana plants using the hydrothermal method (at 180 °C for up to 2 h) with a QY of 48%. Abdullah Issa et al. (2019) on the other hand, synthesized nitrogen doped CQDs (N@CQDs) possessing 3.4 nm size from carboxymethyl cellulose and linear-polyethyleneimine (LPEI). They used a simple hydrothermal method under 260 °C for 2 h and estimated QY to be 44%. Processed white rice waste was used to synthesize CQDs by carbonization method (Anthony et al. 2020). To synthesize the CQDs, a muffle furnace was used to carbonize the powdered sample under 250 °C for 24 h. After 36 h of treatment in an oxidizing environment with stirring at 1200 rpm, the produced CQDs were kept in a reducing environment (with $NaBH_4$) to form reduced CQDs (rCQDs), which were then modified by glutathione (GSH) under stirring. The produced GSH modified rCQDs (GSH@rCQDs) had a size of 2–5 nm and the QY was 41%.

In another study, CQDs were synthesized from orange peel waste via hydrothermal carbonization (Prasannan and Imae 2013). Initially, waste peels were carbonized for 10 h at 150 °C, and then, after a few successive washing stages, hydrothermally heated under 180 °C for 12 h. This procedure yielded CQDs with a 36% QY and a size of 2.7 nm.

Ren et al. (2019) reported that N-doped microporous CQDs (N@mCQDs) can be produced from *Platanus* biomass with a QY of more than 32.4% and an average size of 8 nm via carbonization process carried out at 600 °C for 2 h, under a nitrogenous atmosphere. Then, after a few

Table 1 Summary of various types of QDs developed from different SWs, their developmental methods, and QYs

Type of QDs	Raw material (SW)	Developmental method	QY (%)	Reference
CQDs	Banana pseudo-stem	Hydrothermal	48	(Vandarkuzhali et al. 2017)
	Carboxymethylcellulose	Hydrothermal	44	(Abdullah Issa et al. 2019)
	Orange peels	Hydrothermal	36	(Prasannan and Imae 2013)
	Processed white rice	Carbonization	41	(Anthony et al. 2020)
	Platanus waste	Carbonization	32	(Ren et al. 2019)
GQDs	Waste molasses	Hydrothermal	47	(Sangam et al. 2018)
	Used coffee beans	Hydrothermal	24	(Wang et al. 2016b)
	Alkali lignin	Hydrothermal	21	(Wang et al. 2019b)
	Rice husk biomass	Hydrothermal	8	(Wang et al. 2016c)
	Dead neem leaves	Hydrothermal	2	(Suryawanshi et al. 2014)
	Spent tea	Microwave assisted	23	(Abbas et al. 2020)
	Sugarcane bagasse	Oxidizing cleavage	12.54	(Baweja and Jeet 2019)
GOQDs	Waste toner	Hydrothermal	10.6	(Xu et al. 2019)
	Waste paper	Microwave-assisted, Oxidizing degradation	-	(Adolfsson et al. 2015)

successive stages of heating, a pulsed laser ablation technique was used to get the final product.

Table 1 summarizes SWs-derived CQDs, their developmental methodologies, and QYs. According to literature, most of the SWs generated CQDs have a size of less than 10 nm with average QYs of 30–40%. The low QY of synthesized CQDs is owing to a decrease in fluorescence intensity caused by excessive carbonization and hence CQD aggregation (Alkian et al. 2022).

Synthesis of graphene quantum dots

GQDs have a sheet-like structure, might or might not have functional groups like -OH, -COOH, $-NH_2$, and sulphonic acid group ($-SO_3H$), depending on the synthesis procedure and fabrication. Hence, their solubility depends on the adopted fabrication procedure. Only few studies have reported the detailed synthesis of GQDs using natural and biodegradable SWs as precursors (Abbas et al. 2020; Baweja and Jeet 2019; Ding et al. 2018; Sangam et al. 2018; Suryawanshi et al. 2014; Wang et al. 2016b, 2019b, 2016c), while other types of SWs have never been utilized before. Under various experimental conditions, rice husk, lignin biomass, sugarcane bagasse, tea waste, dead neem leaves, molasses, and coffee grounds were employed to form GQDs of varying sizes. Because there are a limited number of relevant articles, a summary of those works is presented here.

Wang et al. (2016c) successfully synthesized GQDs from rice husk biomass with a yield of 15% (w/w). Rice husk was first processed into rice husk carbon, followed by oxidation with concentrated sulfuric acid and nitric acid. Finally, hydrothermal strategy (200 °C, 10 h) was employed to reduce the 300–500 nm sized rice husk carbon sheet into GQDs of sizes 3–6 nm with 8% QY.

On the other hand, Abbas et al. (2020) used four distinct microwave power sources (100, 300, 500, and 900 W) to synthesize GQDs from tea-waste processed carbon at varying reaction times (15, 30, 60, 120, and 180 min). They observed that the microwave with a power 900 W produces GQDs with a higher conversion rate compared to 500 W. Though the maximum production of GQDs using 900 W was 84% (w/w) (120 min, 7% QY), and the maximum production using 500 W was 84.5% (w/w) (180 min, 23% QY), yields for other time laps were relatively higher in 900 W compared to 500 W power source. Utilizing 500 W and 900 W power separately for 15 min, the isolated yields were only 5% (w/w) and 10% (w/w), respectively. This approach yielded GQDs with average diameter ranging from 5 to 20 nm.

Suryavanshi and co-workers synthesized GQDs from dead neem leaves (Suryawanshi et al. 2014). After processing the dead leaves into black carbon (under an inert environment), it was refluxed at 90 °C for 5 h with a 3:1 mixture of sulfuric and nitric acids to develop GQDs. GQDs were further modified by 30% ammonia solution under hydrothermal conditions, and their average size was found to be ~ 5–6 nm. QYs for GQDs and amine-modified GQDs were determined to be 1% and 2% respectively.

Molasses, a sugar mill waste, was utilized to synthesize sulphur doped GQDs (S@GQDs) through hydrothermal process at 180 °C for 4 h (Sangam et al. 2018). The observed QY was 47% [product yield was 20% (w/w)] and was reported to be the highest QY until then (by using SWs as a source). The Gaussian size distribution of the synthesized S@GQDs was 1.25–3.5 nm. During a study, bagasse, another sugar mill waste, was converted to GO using a modified Hummer's process. Chemical cutting (oxidizing cleavage) was used to synthesis GQDs from the GO (Baweja and Jeet 2019). The QY for the conversion of bagasse to GQDs was 12.54%, and the size distribution was determined to be 5–18 nm.

Wang et al. (2016b) used a hydrothermal technique to synthesize GQDs from discarded coffee grounds. They converted GQDs at 150–200 °C for 6–10 h, with a 33% (w/w) yield. Furthermore, the synthesized GQDs were hydrothermally functionalized with branched polyethyleneimine (bPEI) at 120 °C for 10 h. The highest QY was 24%, and the mean diameters of the GQDs and bPEI functionalized GQDs were 1.88 ± 0.72 and 2.67 ± 0.81 nm, respectively.

GQDs were also prepared from alkali lignin, which is a pulping industry biomass waste (Wang et al. 2019b). Processed black liquid from the Kraft pulping of eucalyptus in the pulp paper industry was treated with concentrated sulfuric acid, to get the alkali lignin. The process of converting alkali lignin to GQDs was divided into two steps: the first was fractionation into lignin nanoparticles doped with nitrogen and sulphur, and the second was a hydrothermal approach to convert the produced lignin nanoparticles into GQDs. As indicated by a dynamic light scattering study, the average diameter range of the synthesized lignin-based GQDs (LGQDs) was 500–800 nm, and the QY was 21% under an excitation wavelength of 380 nm.

In another method, Ding et al. reported the synthesis of GQDs from alkali lignin (Ding et al. 2018). Here, alkali lignin was first treated with 67% nitric acid under ultrasonication to change it into the black carbon-based solution, and the resultant dispersed solution was hydrothermally treated for 12 h at 180 °C. The size range of GQDs was found to be 2–6 nm with a QY of 21%.

Table 1 displays different approaches for synthesizing GQDs from various SWs precursors. The top-down technique for GQD synthesis requires a certain type of carbon skeleton in the starting material, making it less prevalent than CQDs (Zhao et al. 2020). Since majority of SWs lack this sort of structure, therefore mostly GQDs have lower QY than CQDs.

Synthesis of graphene oxide quantum dots

Unlike CQDs and GQDs, GOQDs are produced under a strong oxidizing environment, hence a large number of COOH, -OH, and epoxy functional groups are usually available on their surfaces, making them highly water soluble (Kang et al. 2019). To the best of our knowledge, GOQDs have been reported to be synthesized from waste toner (Xu et al. 2019) and waste paper as SWs sources (Adolfsson et al. 2015) only.

Xu et al. (2019) hydrothermally synthesized GOQDs from waste toner at 180 °C for 4 h in an oxidizing atmosphere of 5% (w/w) hydrogen peroxide. They optimized the experimental conditions to achieve the best results. They further modified the synthesized GOQDs by heating them with polyethyleneimine (PEI) at 60 °C for 3 h to synthesize PEI@GOQDs. The diameter of the synthesized GOQDs, evaluated by HRTEM, was between 2 and 3.5 nm, and the QY was found to be 10.6% under illumination at 340 nm using quinine sulphate as a reference.

Adolfsson et al. developed a microwave-assisted method to synthesize GOQDs from cellulose-enriched waste-paper (Adolfsson et al. 2015). They synthesized the GOQDs in two stages: during the first stage, carbon nanospheres (CNs) were synthesized as an intermediate material directly from waste paper, followed by the conversion of CNs to GOQDs during the second stage. The second stage was sub-divided into two parts, the first being the disintegration of CNs and the second being the oxidation-degradation process. Finally, the heating was performed for various durations (30–60 min) to obtain different sizes of GOQDs. For 30 min and 60 min heating, the final HRTEM analyzed sizes for GOQDs were 3 nm and 1 nm, respectively.

Table 1 summarizes the available literature on GOQDs preparation from SWs. Due to the complexity of the synthesis process and the lower fluorescence intensity compared to the other two QDs, there have not been many reports of GOQDs from SWs. However, conjugated GOQDs are progressively gaining popularity among researchers due to the presence of various functional groups in their structure.

Figure 2 summarizes all the current methods of Cb-QDs synthesis from SWs, with hydrothermal being used in most cases. Hydrothermal synthesis is a simple and efficient approach for producing these Cb-QDs, and the QY obtained from this process is often the highest when compared to the other methods. The microwave is the second-best method for producing Cb-QDs. Both methods are environmentally sustainable but expensive. Reflux, sonochemical, pyrolysis, and other processes are still in their early stages and require further development. Some of the existing methods utilize toxic chemicals, while others demand high temperatures conditions. Thus, efforts should be directed toward the development of efficient, eco-friendly, cost-effective and low temperature procedures for producing Cb-QDs from SWs.

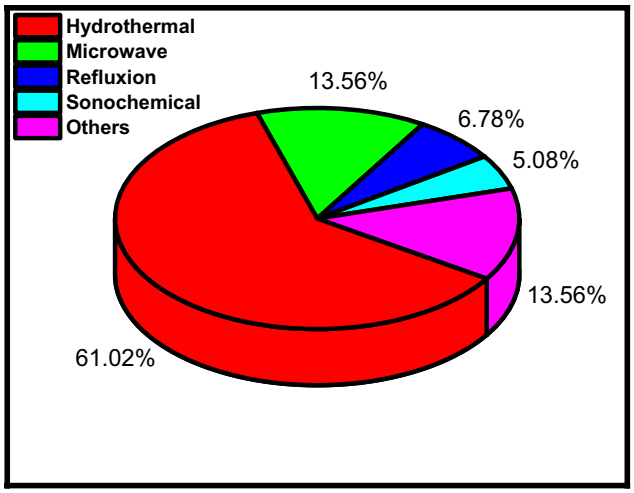

Fig. 2 Various current methods towards the synthesis of Cb-QDs from solid wastes

The temperature of the preparation, the presence of an oxidizing/reducing environment, the structure of starting material's (in some cases), and the synthesis procedure are some vital factors that affect the formation of Cb-QDs. For example, Ye et al. (2013) reported that the size of the GQDs can be tuned by varying the oxidative cutting temperature. They employed a top-down approach (120 °C, under oxidative environment of nitric and sulfuric acids) using bituminous, anthracite, and coke coal as sources. Dong et al. reported that the synthesis of GQDs through the pyrolysis of citric acid followed by carbonization (bottom-up approach) (Dong et al. 2012). The formation of GQDs was found to be dependent on the degree of carbonization, i.e., if the carbonization was incomplete, then the formation of GQDs occurs, while GO is formed when carbonization was complete. Hu and co-workers synthesized GOQDs via oxidation methods using potassium permanganate ($KMnO_4$) and hydrogen peroxide (H_2O_2) separately from graphene (Hu et al. 2018). They had reported that changing the oxidizing agent affect, the structure, fluorescence color, and QY. GOQDs synthesized using H_2O_2, with yellowish green fluorescence (15.1% QY), had a greater number of C–O and C = O bonds than those synthesized with $KMnO_4$ (blue fluorescence and 8.4% QY). Nilewski et al. synthesized GQDs from anthracite and bituminous coal and discovered that bituminous-derived GQDs were 3–5 nm in size compared to 10–20 nm size of GQDs derived from anthracite. Not only their size but their morphologies were also varied (Nilewski et al. 2019). In their procedure, GQDs from anthracite was obtained by keeping the reaction 7 days, while from bituminous, the reaction time was 1 day. The

reason for longer reaction time in case of anthracite is due to the higher inherent graphite like segment compared to that in bituminous (Ye et al. 2013).

Characterization of carbon-based quantum dots

There are three types of characterization methodologies for identifying relevant Cb-QDs:

- Chemical composition or structural characterizations,
- Morphological characterization,
- Optical characterization.

Chemical composition or structural characterizations

Various characterization approaches may be used to identify information about the chemical composition of the QDs and the groups present in various Cb-QDs or functionalized Cb-QDs. Among them, Fourier transform infrared (FT-IR) spectroscopy, X-ray photoelectron spectroscopy (XPS), Raman spectroscopy (RS), energy dispersive X-ray (EDX) analysis, and thermogravimetric analysis (TGA) are most common techniques. Nevertheless, we will limit our discussion only to the characterization of unmodified Cb-QDs as the surface modification will result in many complicated peaks of the spectra.

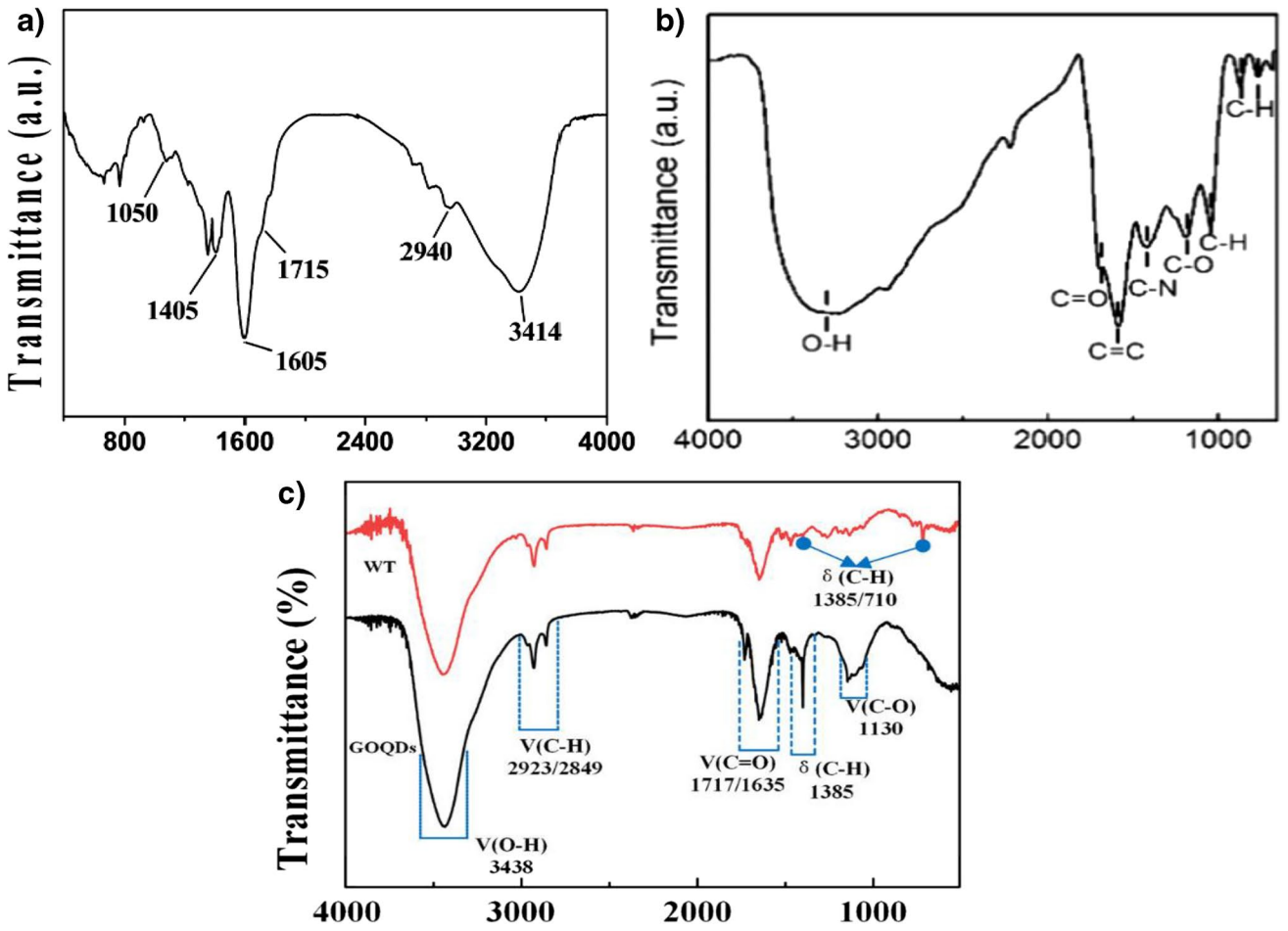

Fig. 3 FTIR spectra of (**a**) lemon peel waste–derived CQDs (Tyagi et al. 2016), (**b**) lignin biomass–derived GQDs (Ding et al. 2018), and (**c**) waste toner–derived GOQDs (Xu et al. 2019)

Fourier transform infrared (FT-IR) analysis

For CQDs The FT-IR analysis data of CQDs prepared from lemon peel waste is shown in Fig. 3a (Tyagi et al. 2016). A broad peak at 3414 cm^{-1} was found in this FT-IR spectrum, which might be due to O–H stretching for water in CQDs. The vibrational frequency of C–H was found to be 2940 cm^{-1}, C = O stretching was observed at 1715 cm^{-1}, and the $-COO^-$ exhibited two peaks at 1605 and 1405 cm^{-1}.

For GQDs GQDs, on the other hand, produce more distinct peaks in FT-IR spectrum than GOQDs (Fig. 3b). Stretching vibration of C = C (for aromatic ring) was detected at 1590 cm^{-1}. The vibrational frequencies of in-plane and out-plane C–H (aromatic) groups appeared at 1041, 870, and 762 cm^{-1}. The presence of O–H, C = O, and C–O groups throughout the periphery of each GQDs sheet resulted in broad maxima at 3360, 1697, and 1190 cm^{-1}. Ding et al. reported that the peak for C–O–C at 1261 cm^{-1} in the starting materials (alkali lignin) was missing in GQDs and it was replaced by a C–N bond (due to nitric acid oxidation), which appeared at 1149 cm^{-1}(Ding et al. 2018).

For GOQDs GOQDs are rich in oxygen containing functional groups on its surface, so due to that polar crown, GOQDs were highly dispersible in water. In FT-IR spectrum for uncoated GOQDs (Fig. 3c), O–H group on the GOQDs surface (or from the water) appeared at 3438 cm^{-1} and two weak C–H bending peaks were found at 2923 and 2849 cm^{-1}. Moreover, one weak and one strong C = O stretching frequency were obtained at 1717 and 1635 cm^{-1}, a weak C–H bending vibration was reported to be at 1385 cm^{-1} in addition to a broad and quite strong type of C–OH stretching frequency (Xu et al. 2019).

X-ray photoelectron spectrum (XPS) analysis

XPS determines the energy of the bonds present on the Cb-QDs. This provides information related to types of the bonding present (i.e., C–O, C = O, C = C, C–O–C) over the specific Cb-QD.

For CQDs Prasannan and Imae (2013) described XPS of orange waste peel–derived CQDs to confirm the various functional groups. The C1s spectral analysis (Fig. 4a) exhibited total of five peaks at 284.9, 285.9, 287.3, and 288.8 eV, respectively for the C = C/C–C, C–OH/C–O–C, C = O, and O = C–O groups. On the other hand, three peaks were found from O1s spectrum (Fig. 4b), at 530.5, 531.9, and 533.2 eV for C–O, C = O, and C–OH/C–O–C species, respectively.

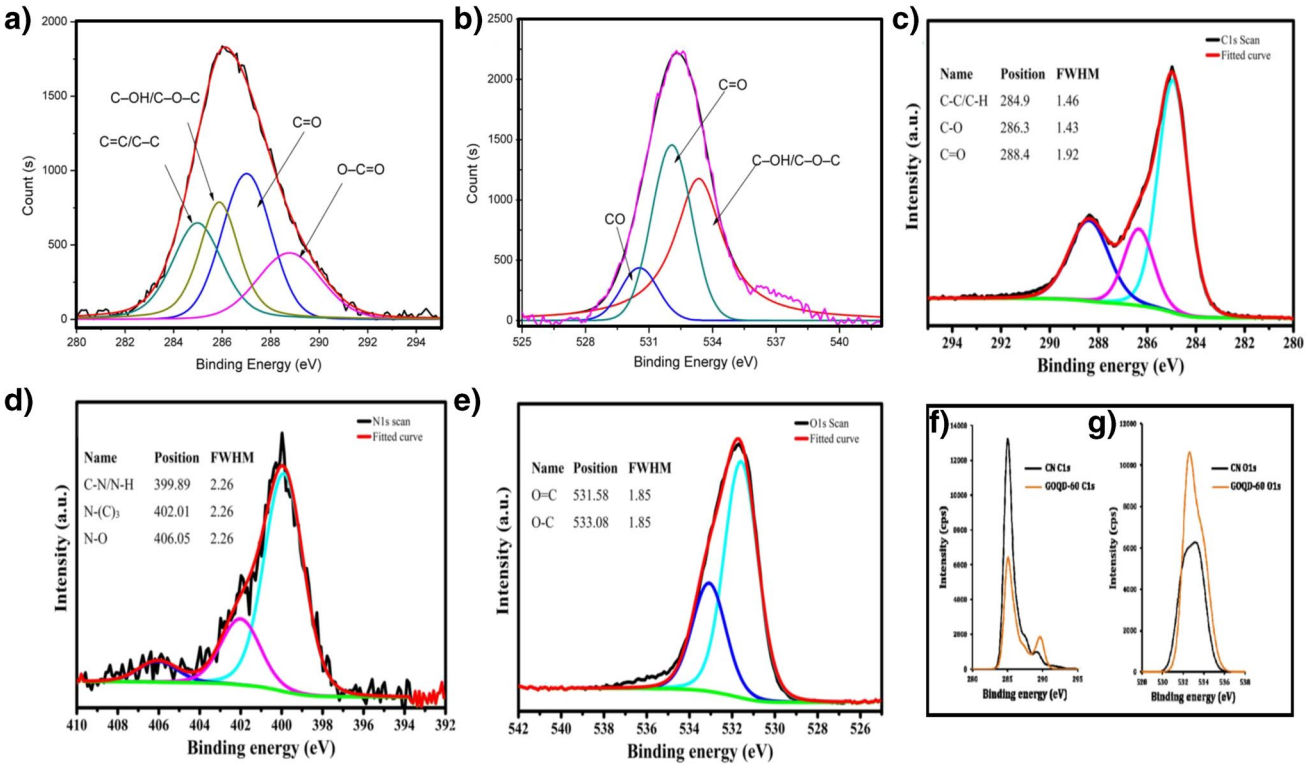

Fig. 4 XPS-spectra of (**a**) C1s and (**b**) O1s type of CQDs, derived from orange waste peel (Prasannan and Imae 2013); (**c**) C1s, (**d**) N1s, and (**e**) O1s of GQDs-derived from spent tea (Abbas et al. 2020); (**f**) C1s, and (**g**) O1s are the and part of the XPS spectra in case of carboxymethyl cellulose–derived GOQDs (Adolfsson et al. 2015)

For GQDs The XPS spectra for the spent tea–derived GQDs showed three peaks at 285.08, 400.08, and 532.08 eV for C1s (Fig. 4c), N1s (Fig. 4d), and O1s (Fig. 4e), respectively, with a small peak at 347.08 eV for Ca 2p (Abbas et al. 2020). The elemental analysis data of GQDs (produced under 500 W) showed C = 56.45%, O = 36.73%, N = 4.76%, and traces of Ca. C1s spectral analysis under high resolution XPS showed that they had three peaks at 284.9, 286.3, and 288.4 eV, for C–C/C = C, C–O–C, and O-C = O groups. N1s spectral analysis revealed three peaks at 399.89, 402.01, and 406.05 eV, for C–N/N–H (pyridinic or pyrrolic), N–C (3°-amine), and N–O (nitro) bonds, respectively. O1s spectrum on the other hand possessed two peaks at 531.58 and 533.08 eV, for O = C and O–C species, respectively. They also found that no structural change occurred in GQDs after 2 months, demonstrating excellent GQDs stability.

For GOQDs The XPS C1s spectral analysis (Fig. 4f) of carbon nanospheres showed four peaks at 285 (C–C/C = C), 286.3 (C–O), 287.5 (C–O–C), 289.2 (O = C–O), and 290.1 eV (π-π* of aromatic ring) and three for GOQDs, viz. 285 (C–C/C = C), 286 (C–O), 287.3 (C–O–C), and 288.3 eV (O = C–O), respectively (Adolfsson et al. 2015), while two O1s spectral analysis peaks (Fig. 4g) were found at 532 and 533.4 eV for C = O and C–O groups. After the conversion of CNs to GOQDs, the increase in oxygen containing groups can be attributed to the decrease in C/O ratio from 4.2 to 2.0.

All three types of Cb-QDs might contain similar or different types of groups, depending on the synthetic procedures. If highly polar groups (e.g., COOH, C = O, OH, N–H) are present at the edge or exterior surface of the Cb-QDs, then those QDs would be highly soluble in water. With modification, we can tune the solubility as well as other properties of the QDs.

Miscellaneous skeletal characterizations

Other characterization techniques include RS, EDX analysis, TGA analysis, solid state cross polarization/magnetic angle spinning ^{13}C nuclear magnetic resonance spectroscopy (CP-MAS-^{13}C-NMR) analysis, two-dimensional NMR (2D-NMR) analysis, heteronuclear single quantum coherence (HSQC) spectroscopic analysis, gas chromatography–mass spectrometry (GC–MS), and high-performance liquid chromatography (HPLC).

Like FT-IR, RS detects the functional groups present over Cb-QDs. Although RS is more time consuming and expensive than FT-IR, it has the advantage of not being affected by the presence of water molecules in the spectra. The CP-MAS-^{13}C-NMR spectra can distinguish between processed and unprocessed materials (David et al. 2009). When compared to 1D-NMR, 2D-NMR provides more information on the type of protonic environment, but HSQC provides information about proton coupling with heteronuclei, i.e., we may find out the interaction of a proton and a heteronuclei using this form of NMR spectroscopy. The elemental composition of the various QDs is determined using EDX analysis. TGA confirms the deposition of various molecules, drugs, or nanomaterials on the surface of Cb-QDs sheet. GC–MS identifies the components in QDs from the starting materials/final products mixtures and clearly reveals about whether the conversion is completed or not. Unlike GC–MS, HPLC can detect the components from the same mixtures but in the liquid phase and with varied time intervals.

Morphological analysis

For morphological analysis, the preferential characterization technique is transmission electron microscopy (TEM) and its high-resolution version (HRTEM), which simultaneously furnishes the details about size, shape, layers, and thickness. Morphological analysis is discussed below for the three unmodified Cb-QDs.

Transmission electron microscopy (TEM) analysis

The CQDs synthesized from peanut shell were analyzed by TEM (Xue et al. 2016). The CQDs were spherical in shape with 2–4 nm diameter (Fig. 5a). From single crystalline structural analysis by HRTEM, the lattice spacing was estimated to be 0.338 nm (Fig. 5b), corresponding to the (002) graphitic plane.

In one study, HRTEM, employed for rice husk–derived GQDs analysis indicated its highly crystalline nature with spacing of 0.24 nm i.e., (1120) diffraction plane (Fig. 5c) (Wang et al. 2016b). TEM analysis of the GQDs revealed the size range 3–6 nm (Fig. 5d).

Xu et al. (2019) reported that the GOQDs produced from waste toner had a size range of 2 – 3.5 nm (histogram, Fig. 5f) using TEM analysis (Fig. 5e). The space in a single GOQDs crystal was estimated to be roughly 0.2 nm using HRTEM, resulting in a (102) plane of diffraction (graphitic sp^2 carbon, JCPDS no.- 26–1076) (Fig. 5g).

Miscellaneous techniques related to morphological analysis

Dynamic light scattering (DLS) data partially offers an idea of the size of the QDs. Scanning electron microscopy (SEM) and atomic force microscopy (AFM) are also used to analyze the morphology of diverse nanomaterials, which includes the size, shape, thickness of the layers, and surface stability. To confirm the structures of crystalline nanomaterials, powder X-ray diffractometry (XRD) is used. Selected area electron diffraction (SAED) pattern is employed to

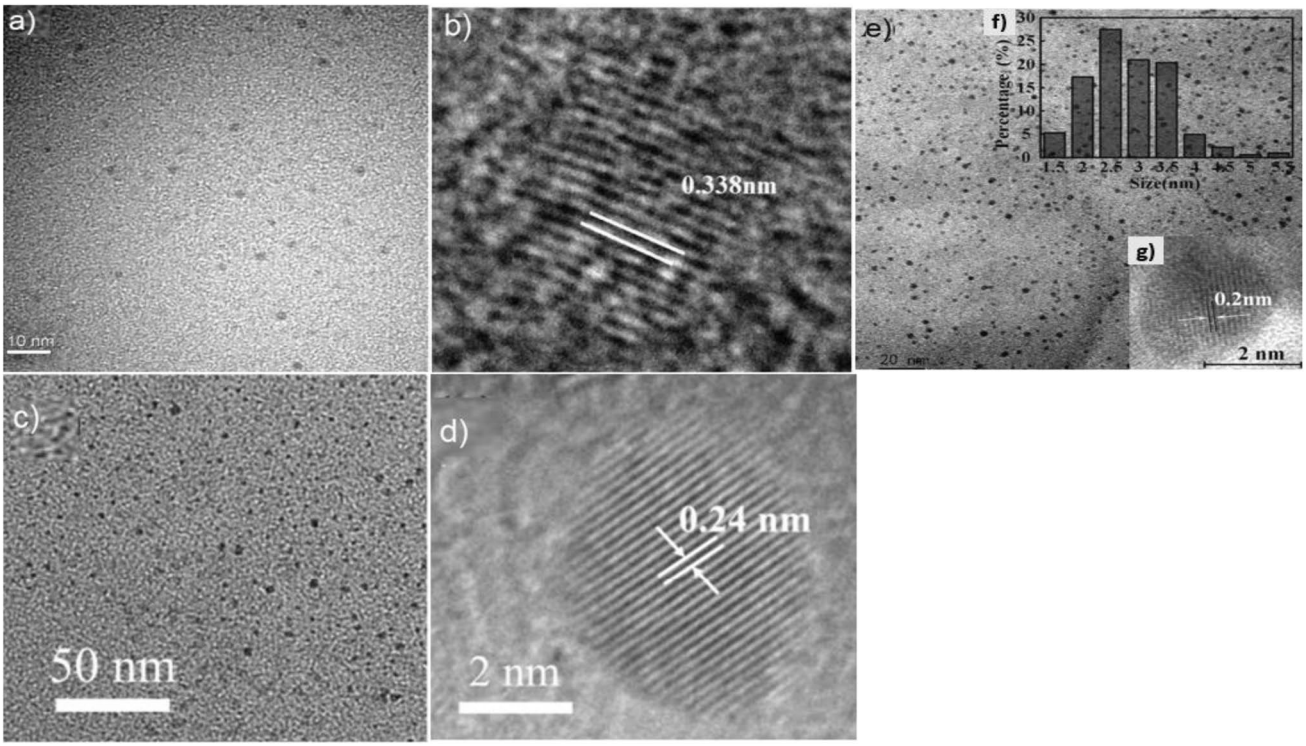

Fig. 5 TEM image (resolution 10 nm) (**a**) and corresponding HRTEM of a single CQDs crystal of peanut shell–derived CQDs (**b**) (Xue et al. 2016); TEM (resolution 50 nm) (**c**) and HRTEM (2 nm) images of rice husk–derived GQDs (**d**) (Wang et al. 2016c); TEM (resolution 20 nm) (**e**), corresponding size analysis histogram (**f**) (inset) and HRTEM (2 nm) image (**g**) (inset) of waste toner–derived GOQDs (Xu et al. 2019)

validate the crystallinity data obtained by powder XRD. Brunauer–Emmett–Teller (BET) surface area analysis explores the specific surface area (in m^2/g) of Cb-QDs via gas (inert type, viz. nitrogen) adsorption analysis, over a solid sample.

Optical characterization analysis

UV–visible and photoluminescence spectral analysis

UV–Visible spectroscopy is one of the most effective tools to obtain preliminary information for the efficient fluorescence characteristics of Cb-QDs. Furthermore, the presence of conjugation or electron excessive groups/atoms on the QDs can be concluded by UV–Vis spectral analysis (Table 2). Photoluminescence (PL) spectroscopy is used to examine the fluorescence and phosphorescence abilities of QDs, as well as the QY, which indicates the successful conversion of a carbon source into QDs, at a maximum excitation wavelength (Table 2).

According to Wang and Hu (2014), the color of fluorescence varies with the size of CQDs. The red shift for emissive radiation occurs when the size of Cb-QDs increases, due to a decrease in the HOMO–LUMO gap.

Miscellaneous optical characterizations

There are a variety of different optical techniques that can be used to fully comprehend the fluorescence properties of QDs. Time-correlated photon counting (TCSPC) is an optical characterization technique that measures the fluorescence decays and directly tells us about the lifetime of a QDs. Time-resolved photoluminescence (TRPL) is an extension of normal fluorescence spectroscopy that produces an excitation spectrum as a function of time. Furthermore, Fluorocube time-correlated single photon counting (TCSPC) fluorimetry is a well-developed method of measuring fluorescence lifetime with high data accuracy and high sensitivity.

Based on all the characterization techniques, the following conclusions can be drawn:

- UV–Vis, PL, XPS, EDX, and FTIR spectroscopy can be used to identify all three Cb-QDs.
- Carbon sheets are organized into layers to form a complete spherical CQD crystal, whereas GQDs and GOQDs exhibit a sheet-like structure.
- CQDs and GQDs are generally less polar than GOQDs, regardless of modification, and so the latter have distinct water solubility.

Table 2 Summary of UV–visible and photoluminescence spectroscopic data for the reported SWs-derived Cb-QDs

Raw material	UV–Vis finding (nm)	PL max. intensity (nm)	Reference
CQDs			
Banana pseudo-stem	284 ($\pi \rightarrow \pi^*$, C = C)	340	(Vandarkuzhali et al. 2017)
Carboxymethyl cellulose	294 ($\pi \rightarrow \pi^*$, C = C) 312 and 350 ($n \rightarrow \pi^*$ of C = O in CQDs and N@CQDs)	350	(Abdullah Issa et al. 2019)
Processed white rice	340 ($n \rightarrow \pi^*$)	345	(Anthony et al. 2020)
Orange peels	268 ($\pi \rightarrow \pi^*$)	340	(Prasannan and Imae 2013)
Platanus waste	295 ($\pi \rightarrow \pi^*$) 389 ($n \rightarrow \pi^*$)	390	(Ren et al. 2019)
GQDs			
Rice husk biomass	-	335	(Wang et al. 2016c)
Spent tea	300 ($n \rightarrow \pi^*$)	340	(Abbas et al. 2020)
Dead neem leaves	300 ($n \rightarrow \pi^*$) < 300 ($\pi \rightarrow \pi^*$)	350	(Suryawanshi et al. 2014)
Alkali lignin	238 ($\pi \rightarrow \pi^*$, C = C/C = N) 295 ($\pi \rightarrow \pi^*$, lignin-derived sp^2 aromatic domain)	380	(Wang et al. 2019b)
Waste molasses	270 ($\pi \rightarrow \pi^*$) 300 ($n \rightarrow \pi^*$)	340	(Sangam et al. 2018)
Sugarcane bagasse	280 ($\pi \rightarrow \pi^*$) 330 ($n \rightarrow \pi^*$)	435	(Baweja and Jeet 2019)
Used coffee beans	-	390	(Wang et al. 2016b)
Alkali lignin	280 ($\pi \rightarrow \pi^*$) 350 ($n \rightarrow \pi^*$)	310	(Ding et al. 2018)
GOQDs			
Waste toner	235 ($\pi \rightarrow \pi^*$, C = C) 280 ($n \rightarrow \pi^*$, C = O) 340 nm (surface of GOQDs)	340	(Xu et al. 2019)
Waste paper	200 ($\pi \rightarrow \pi^*$, C = C) 320 ($n \rightarrow \pi^*$, C = O)	330	(Adolfsson et al. 2015)

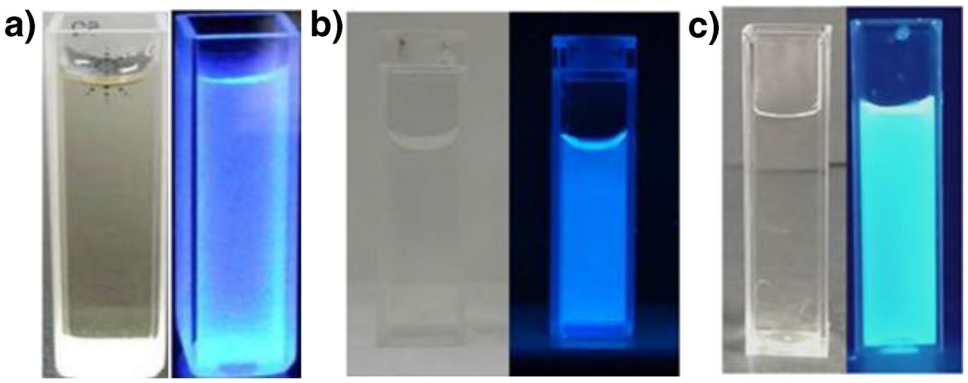

Fig. 6 (**a**) Peanut shell–derived CQDs before excitation (left) and after excitation at 365 nm (right) (Xue et al. 2016); (**b**) GQDs from rice husk biomass under visible (left) and at 365 nm UV irradiation (right) (Wang et al. 2016c); (**c**) waste toner–derived GOQDs under day light (left) and 365 nm UV irradiation (right) (Xu et al. 2019)

- CQDs and GQDs, on average, have a higher C/O ratio than GOQDs.
- When exposed to UV light, all three types of Cb-QDs emit light at the same frequency for example, blue emission occurs for all three types of Cb-QDs at 365 nm (Fig. 6).
- All the three types of Cb-QDs would have the same surface functionalities if they were synthesized from the same carbon source.
- In CQDs and GQDs, the numbers of conjugated mobile (π-bonded) electrons are higher than in GOQDs. As a result, GOQDs are not probably exploited as popular fluorescent materials.

Applications of carbon-based quantum dots

Cb-QDs, with and without surface functionalization, have gained immense attention among researchers in the past decades due to their wide range of applications. Because of their small size and perfect shape, they are used in various areas like bioimaging, in vitro sensing, drug delivery, chemical sensing, environmental applications, electrical devices, and catalysis. Herein, the various applications of Cb-QDs derived from SWs in the fields of biomedicine, electrical devices, environmental, and catalysis are discussed.

Biomedical applications

Cytotoxicity is a serious issue in the development of medications and therapeutic procedures since it can have a negative impact on both infected and normal tissues. Cb-QDs are now emerging as one of the important materials for biomedical applications because of their lower toxicity than other inorganic-based QDs. Cb-CDs at various concentrations, with or without surface modifications or doping, have been shown to be less cytotoxic, and thus more biocompatible on various cell lines. CQDs derived from alkali lignin showed more than 83% viability of HeLa cell lines even after 24 h incubation with a dosage of 50 mg/L (Zhang et al. 2019). Similarly, the cell viability of HeLa cells was above 90% when incubated with a high concentration of waste frying oil–derived sulphur-doped CQDs (600 µg/L) for 48 h. Likewise, a higher concentration of CQDs (1 mg/L) from the pseudo-stem of a banana plant on incubation with Hela and MCF-7 cell lines for 24 h revealed more than 85% cell viability. Similar types of high cell viability were observed for other cell lines (like A549, HepG2, Vero, HCT116, C6, T24) even after incubation for ≥ 24 h with a higher concentration of functionalized/doped/uncoated CQDs (Table 3). Like CQDs, functionalized/doped/uncoated GQDs also showed similar types of HeLa, L929, 3T3, HepG2, HEK293, etc., cell viability when incubated for ≥ 24 h. There is no information on the cytotoxicity of SWs-derived GOQDs on any types of cells. A live-cell imaging and sensing of cholesterol is illustrated in Fig. 7.

Drug delivery, sensors, magnetic hypothermia, photothermal therapy, in vivo imaging, and in vitro biosensing are currently well-developed techniques with Cb-QDs. Despite the fact that a nanomaterial's ability to penetrate the blood–brain barrier (BBB) is challenging, several articles have reported that the relevant Cb-QDs can be effective in overcoming the problem. Kim et al. (2018) synthesized unfunctionalized GQDs and showed their ability to prevent synucleinopathy in Parkinson's disease. Because of the strong fluorescence, water solubility, photo-stability, low toxicity, cell-membrane permeability, and excellent biocompatibility, CQDs produced from the pseudo-stem of the banana plant were used as fluorescent probes for imaging of HeLa and MCF-7 cells in three colors (blue, green, and red) (Vandarkuzhali et al. 2017). The highly luminous r-CQDs-GS from processed white rice has been effectively proven for in vitro and in vivo bioimaging of A549 cells (Anthony et al. 2020). Apart from that, fabricated N-doped CQDs derived from *Platanus* biomass have been widely used for cellular imaging of HeLa cells, L02 cells, and macrophage cells. There are other reports where CQDs derived from SWs were used for imaging different carcinoma cells like HeLa, C6, MC3T3 HUVEC, MDA-MB-231, Caco-2, DU145, and more (Zhang et al. 2019). Apart from biosensing of cells, fluorescent CQDs from diesel engine soot have been successfully utilized for the imaging of *Escherichia coli* (*E. Coli*) along with the sensing of cholesterol (Tripathi et al. 2014). Several other researchers have used SWs-derived CQDs for a variety of other applications, including bacterial cell imaging (Ang et al. 2020; Tripathi et al. 2014), drug sensing (Yu et al. 2019), drug delivery (D'souza et al. 2018), and antioxidant (Rajamanikandan et al. 2021). Unlike CQDs, applications of GQDs derived from SWs are yet to be explored in their wider range. Internalization of GQDs derived from waste molasses has also demonstrated in DF-1, HepG2, and HEK293 cells (Sangam et al. 2018). There are studies on the use of GQDs derived from SWs for bioimaging of HeLa (Wang et al. 2016b, 2016c), L929 and 3T3 (Wang et al. 2019a, b) types of cells as well. Until now, there has only been one report where GOQDs derived from toner waste was used to quantify specific DNA sequences from extracts of genetically modified plant tissues (Xu et al. 2019). Table 3 summarizes the biomedical applications of SWs-derived Cb-QDs.

Uncoated Cb-QDs are generally perceived to be biocompatible materials as they do not contain any harmful or toxic substances, however their strong ROS generation ability causes DNA damage (Wang et al. 2015b) and cell damage (Markovic et al. 2012; Wang et al. 2016d). However, many articles suggested that these zero-dimensional materials are safe to the biological systems. For example, Yan et al. reported in an article that, they had synthesized biocompatible GQDs, which are extremely biocompatible compared to the GQDs produced by conventional methods (Yan et al. 2020), Halder et al. also mentioned that their GQDs were biocompatible towards their cellular uptake studies (Halder et al. 2018). Liu et al. investigated an important aspect that whether presence and absence of light to CQDs affects the normal and cancer cells or not (Liu et al. 2021a). Previously reported articles (Bagheri et al. 2018; Meziani et al. 2016; Stanković et al. 2018) suggested that CQDs on irradiation with certain wavelength of light caused the death of bacteria and yeasts. According to Liu et al. (2021a), because prior cytotoxicity studies were conducted in the dark, CQDs

Table 3 Biomedical applications of SWs-derived Cb-QDs

Raw material	Biomedical application	Type of cells, viability, and concentration	Reference
CQDs Banana pseudo-stem	Bioimaging	MCF-7 and Hela 85%, 1 mg/L	(Vandarkuzhali et al. 2017)
Processed white rice	In vitro and in vivo bioimaging	A549 ≥90%, 100 µg/mL	(Anthony et al. 2020)
Platanus waste	Cellular imaging	HeLa ≥83%, 1.2 mg/mL	(Ren et al. 2019)
Diesel engine soot	Imaging of *E.Coli* cells	HepG2 ≥90%, 50 µg/mL	(Tripathi et al. 2014)
Alkali lignin	In vitro bioimaging of Hela cells	HeLa ≥95%, 12.5 mg/mL	(Zhang et al. 2019)
Peanut shell	HepG2 cell imaging	HepG2 ≥90%, 1.2 mg/mL	(Xue et al. 2016)
Crab shell	Bioimaging and drug delivery	HeLa ≥90%, 1000 µg/mL HepG2 ≥90%, 1000 µg/mL HeLung ≥90%, 1000 µg/mL	(Yao et al. 2017)
Waste frying oil	Cellular imaging of Hela cells	HeLa ≥90%, 600 µg/mL	(Hu et al. 2014b)
Waste palm oil	In vitro cytotoxicity within vero cells	Vero CC_{50} 12%	(Mahat and Shamsudin 2020)
Cat feedstock waste	In vitro cellular imaging of HCT116	HCT116 ≥80%, 500 µg/mL	(Ahn et al. 2019)
Ananas comosus peels	Antioxidant activity	—	(Rajamanikandan et al. 2021)
Waste paper	Cellular imaging of C6 cell lines	C6 >90%, 1 mg/mL	(Jeong et al. 2018)
Expired milk	Bioimaging of HeLa cells	HeLa ≥90%, 400 µg/mL	(Su et al. 2018)
Diesel engine soot	Cellular imaging of *E. coli* and sensing cholesterol	—	(Tripathi et al. 2014)
Sugarcane industrial waste	Antimicrobial activity using two-gram positive bacteria (*Bacillus cereus* and *staphylococcus aureus*) and three gram negative (*Pseudomonas aeruginosa* and *Vibrio cholera* and *E. coli*	—	(Pandiyan et al. 2020)
Walnut shell	Intracellular bioimaging using MC_3T_3 cells	MC_3T_3 ≥90%, 100 µg/mL	(Cheng et al. 2017)
Pineapple peel	Intracellular imaging of HeLa and Hg^{2+} detection	HeLa and MCF-7 ≥84%, 1 mg/mL	(Vandarkuzhali et al. 2018)
Palm kernel shell	Cellular imaging of *E. coli* and *B. subtilis*	—	(Ang et al. 2020)
Onion peel powder	Cellular imaging using MG63/HFFs cells, antioxidant study, invitro superoxide inhibition activity study	MG63/HFF ~80%, 2.5 mg/mL	(Bankoti et al. 2017)
Wheat straw	Labelling of $CaCO_3$, bioimaging in *E. coli* cells	—	(Yuan et al. 2015)
Wheat straw	Cellular imaging using HeLa cell	HeLa >95%, 800 µg/mL	(Liu et al. 2021b)
Tea waste	In vitro Antioxidant study	N.A	(Chen et al. 2019)
Cow manure	Staining to the MCF-7, HUVEC, MDA-MB-231, Caco-2, and DU145 cells	MCF-7, HUVEC, MDA-MB-231, Caco-2, DU145 >95%	(D'Angelis do E. S. Barbosa et al. 2015)

Table 3 (continued)

Raw material	Biomedical application	Type of cells, viability, and concentration	Reference
Egg shell	Fluorescent probe for label free binding to both natural and synthetic DNAs	—	(Pramanik et al. 2018)
Cow manure	Detection of Glucose, immunotherapeutic agent for melanoma skin cancer	B16F10,NIH3T3 >80%, 0.1 mg/mL	(Horst et al. 2021)
Waste paper	Bioimaging using C6 cells	C6 90%, 1 mg/mL	(Jeong et al. 2018)
Daucus carota subsp. Sativus root	Cellular imaging of *Bacillus subtilis* and drug (mitomycin) delivery	MCF-7 ≥95%, 1000 µg/mL	(D'souza et al. 2018)
Lotus root	Off–on fluorescence nanosensor for determination of 6-thioguanine in plasma and urine of leukemia patient and its bioimaging in living cells	T24 ≥90%, 1200 µg/mL	(Yu et al. 2019)
GQDs			
Waste molasses	Bioimaging	DF-1, 92%, 2 mg/mL HEK293 95%, 2 mg/mL HepG2 88%, 2 mg/mL	(Sangam et al. 2018)
Used coffee beans	Bioimaging and sensing	HeLa ≥88%, 40 mg/mL ≥62%, 160 mg/mL	(Wang et al. 2016b)
Alkali lignin	Physiological oxidant	L929 and 3T3 ≥90%, 100 µg/mL	(Wang et al. 2019b)
Rice husk	Cellular imaging	HeLa ≥90%, 100 µg/mL	(Wang et al. 2016c)
GOQDs			
Waste toner	Fluorometric DNA hybridization	—	(Xu et al. 2019)

were shown to be an exceptionally biocompatible material; however, in present days of experiments, fluorescent images are taken by using certain wavelength of light. Hence, they investigated the effect of irradiation on the normal (HEK-293 kidney epithelial cells) and cancer-cells (HeLa cervical cancer cells and HepG2 hepatocellular carcinoma cells) and observed that the generated ROS damage occurs to both types of cells.

The Cb-QDs are smaller and composed of C, O, and H-based (and sometimes S and N-based) components, therefore it is unlikely that they would be toxic to living organisms. However further research in this area is necessary, as these Cb-QDs are not until now entirely safe for use in biological applications.

Energy storage and electronic device related applications

Higher electrical conductivity, larger surface area, better solubility in many solvents, enhanced photoluminescence, excellent mobility, and adjustable band gap are only a few of the significant physicochemical features that are preferential requirements for the usability of Cb-QDs towards electronic devices such as photovoltaic devices, light-emitting diodes, solar cells, fuel cells, batteries, and supercapacitors. However, the energy applications of Cb-QDs derived from SWs precursors have yet to be developed. Surendran et al. (2020) used Z-scan analysis to apply the orange waste peel–derived CQDs in optical switching photonic devices. Park et al. (2020) synthesized CQDs from waste paper and utilized them to make anti-counterfeiting ink and flexible display. Athika and co-worker utilized expired milk for the synthesis of CQDs, which have been used as supercapacitors with > 1000 charge/discharge cycles of columbic efficiency (Athika et al. 2019). Vandarkuzhali et al. (2018) demonstrated that the pineapple peel-derived CQDs can be used for electronic security devices and memory devices. Liu et al. (2014) created a 2D pattern using human hair–derived CQDs, which is visible under UV light (Fig. 8).

Recently, CQDs have received immense attention due to their improved solubility and surface tenability, yet a few SWs-derived CQDs are employed in device applications. Moreover, bulk scale syntheses for GQDs and GOQDs have

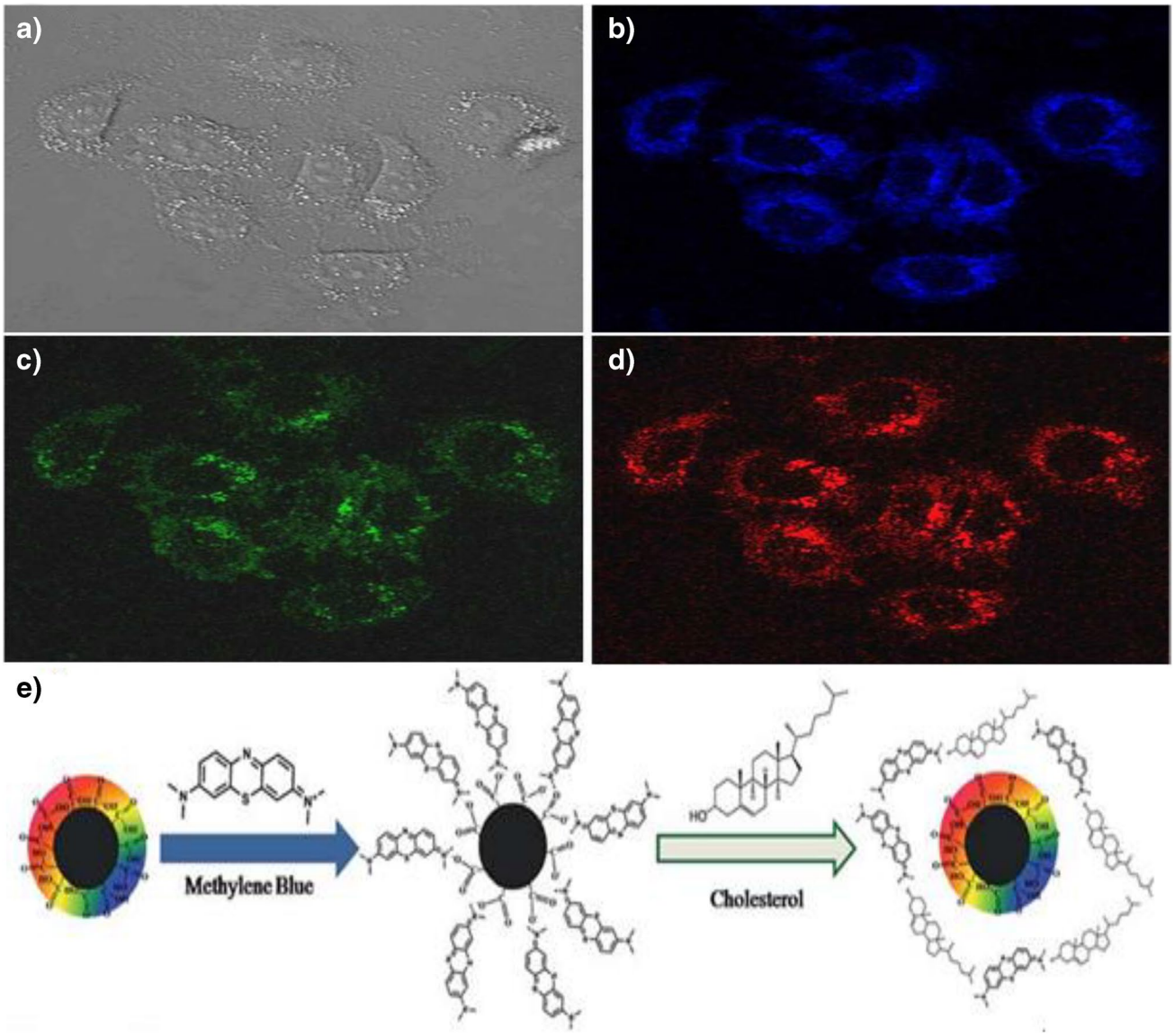

Fig. 7 Living cell imaging in case of HepG2 cells incubated with CQDs at 37 °C. (**a**) Bright field and fluorescent image under excitation with laser at (**b**) 405 nm, (**c**) 488 nm, and (**d**) 514 nm.(Xue et al. 2016); (**e**) sensing scheme of cholesterol by diesel soot–derived CQDs (Tripathi et al. 2014)

yet to be developed as the existing approaches produced relatively low QY.

Environmental and catalytic applications

Sensing and adsorption of environmentally hazardous chemical compounds including heavy metal ions are included in this category (Ng et al. 2021). CQDs and GQDs with no or few polar groups are not beneficial in environmental applications, because they poorly dispersed in polar solvent such as water and ethanol (Yoo et al. 2019). As a result, emphasis must be placed on the expansion of the highly polar groups to utilize them in environmental application.

To date, SWs-derived Cb-QDs have been applied towards the detection of Cu^{2+} (Abdullah Issa et al., 2019; Ang et al. 2020; Gedda et al. 2016; Venkatesan et al. 2019; Y. Wang et al. 2015a), Fe^{3+} (Abbas et al. 2020; Ahn et al. 2019; Chen et al. 2019; Liu et al. 2015; Su et al. 2018; Vandarkuzhali et al. 2017; Venkatesan et al. 2019; Wang et al. 2020; Ye et al. 2017; Yuan et al. 2015), Cr^{6+} (Athika et al. 2019; D. et al. 2019; Tyagi et al. 2016), Hg^{2+} (Guo et al. 2016; Xu-Cheng et al. 2018; Ye et al. 2017, 2020), CrO_4^{2-} (Chen et al. 2019), F^- (Liu et al. 2021a, b), GSH (Wang et al. 2012), selenite (Devi et al. 2017), tetrazine (Thulasi et al. 2020), nitro-explosives (Devi et al. 2018), picric acid (Venkatesan et al. 2019), L-cysteine (Chen et al. 2019), ascorbic

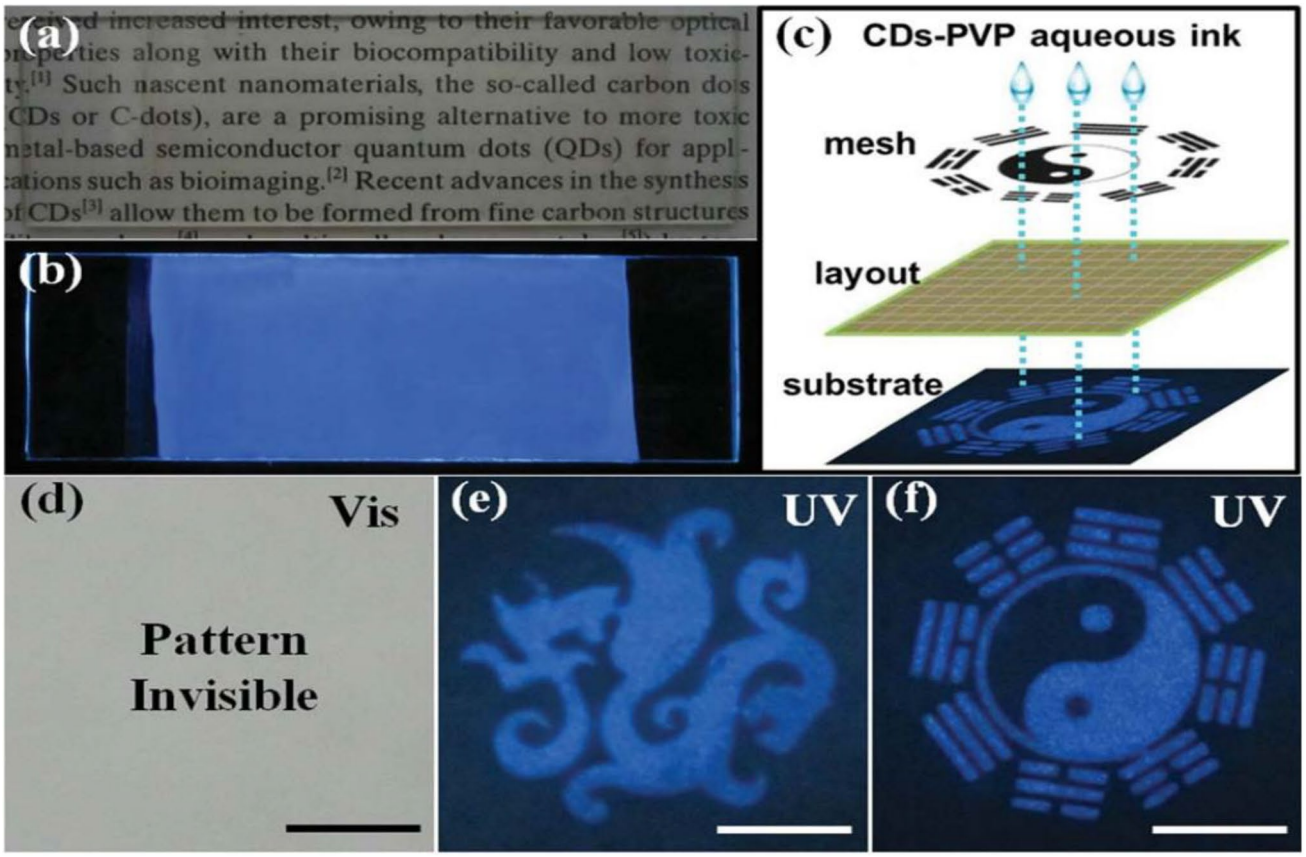

Fig. 8 Hair-derived CQDs based fluorescent film under (**a**) daylight and (**b**) UV irradiation; (**c**) silk screen printing illustration scheme; (**d**) and (**e**) and (**f**) are the fluorescent 2D patterns by CQDs solution under day light and UV light, respectively (Liu et al. 2014)

acid (Chen et al. 2019), and chloroform (Singh et al. 2020). CQDs derived from dead neem leaves were applied towards making a probe for Ag^{+} ions detection (Suryawanshi et al. 2014). Hu et al. (2021) on the other hand reported an application for orange peel–derived CQDs in the the detection of *E. coli* in milk.

According to WHO and other environmental agencies (EPA and USPEA), Cu^{2+}, Fe^{3+}, Cr^{6+}, Hg^{2+}, selenium, F^{-} ions, and chloroform concentrations in drinking water should be less than 1.3, 0.3, 0.01, 0.002, 0.05, 4.0, and 0.3 mg/L, respectively, (Adebayo 2011; Chromium in Drinking Water | US EPA n.d.; National Primary Drinking Water Regulations | US EPA n.d; "Selenium in Drinking-water Background document for development of WHO Guidelines for Drinking-water Quality" 2011; Devi et al. 2017; Raber 1998). Exposure beyond this threshold can result in gastrointestinal upset, liver damage, central nervous system disorders, or renal damage, among other things. Cb-QDs made from SWs can detect all these ions below their safe limits. Apart from that, Cb-QDs may also detect organic compounds such as tetrazine (an artificial food color), picric acid, amino acids, and chloroform below their acceptable limit. As a result, the presence and the amount of these hazardous and toxic materials must be carefully determined to ensure a lower risk. For this purpose, Cb-QDs and their modified form can help in a simple and better way with minimum cost.

The carbon-based semiconductors are also useful as catalysts in reactions and photolysis. Prasannan and Imae (2013) synthesized CQDs from orange peels and, after combining them with ZnO, used them for photocatalytic degradation of naphthol blue-black, an azo dye (Fig. 9). In another work, Tyagi et al. (2016) used lemon peel–derived CQDs (after modification with TiO_2) for photocatalytic degradation of methylene blue. However, because of poor conversion yield, the catalytic applications of SWs-derived Cb-QDs are rare. We have included some representative papers related to SWs-derived Cb-QDs and their respective environmental applications, along with catalytic applications with experimental data in Table 4.

In few works, during the detection of metal ion by those Cb-QDs, LOD values were found in the nanomolar (nM) range, which shows better efficiency. Whereas, in most of the cases LOD values were found in the micromolar (μM) or ppb level, which should be improved. Similar to other applications, CQDs are most preferable here over, owing to their intense fluorescence property.

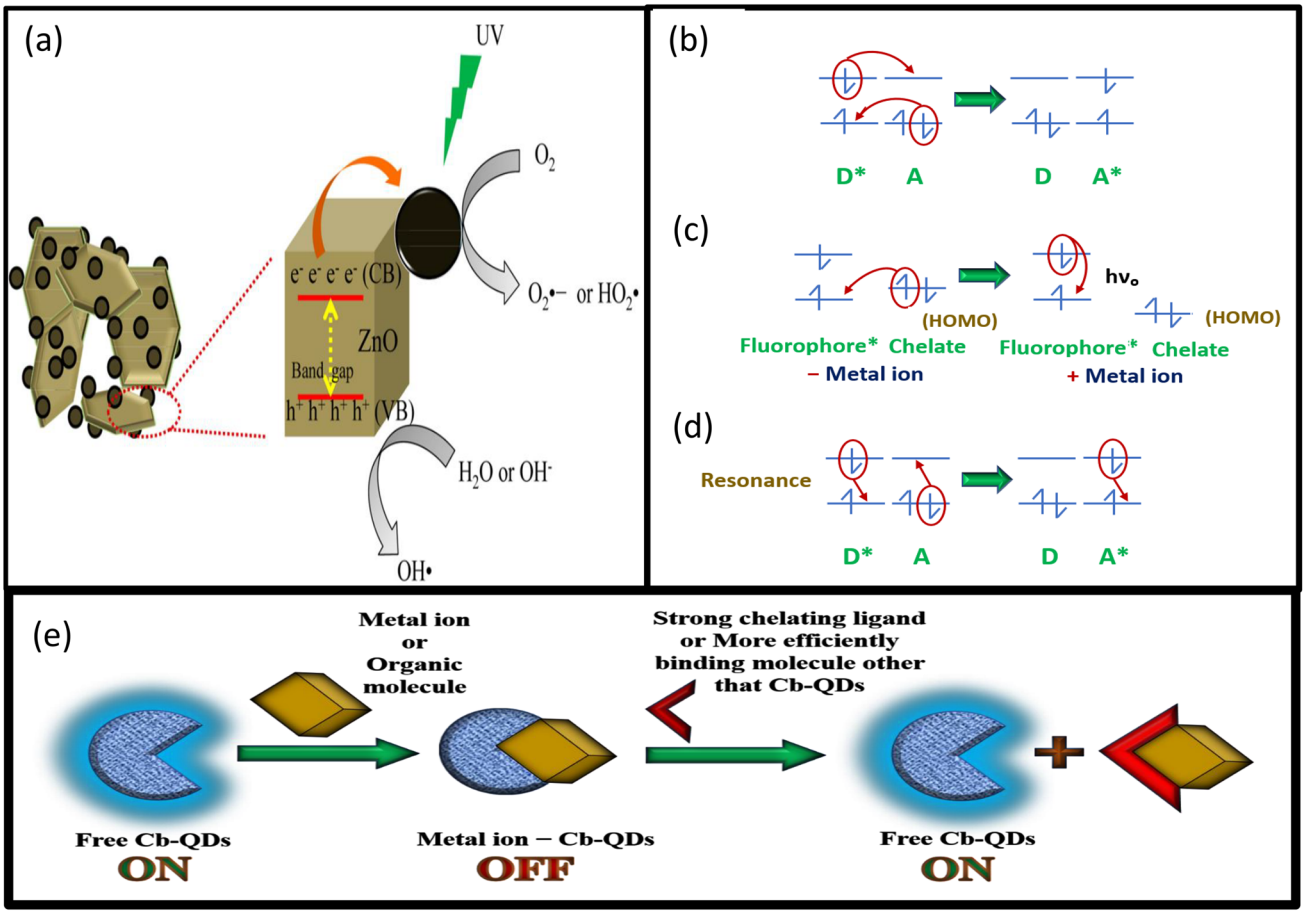

Fig. 9 Orange waste peel–derived CQDs as UV light acceptor in CQDs@ZnO nanocomposite towards the degradation of naphthol blue-black dye (**a**) (Prasannan and Imae 2013), Dexter energy transfer (**b**), PET (**c**), and FRET (**d**) mechanism of sensing (Skourtis et al. 2016), and "on–off-on" process of metal ion and organic compound sensing (**e**)

Sensing and imaging mechanism of Cb-QDs

Fluorescent materials have the special ability to emit light after the absorption of a particular wavelength of incident irradiation. A fluorescence microscope is used to measure the alteration of that particular wavelength. Every fluorescent sensing material must have the binding sites (chelating type) and at least one fluorophore (capable of absorption and emission of light). If the binding of a particular metal ion or organic compound to that sensing material causes the alteration of the electronic environment and/or molecular structure, then only a fluorescent microscope can visualize or sense that metal ion or organic compound. The modulation of electronic structure between the metal ion or organic compound and the fluorophore can be described by three simple mechanisms: Dextar, photoinduced electron transfer (PET), and Forster resonance energy transfer (FRET). The effects of electron or energy transfer between the metal ion or organic compound and the fluorophore, results in a "turn-off" (decreased or no) or "turn-on" (increased) fluorescence response.

In the first type of mechanism, energy transfer (quenching) can occur via the Dexter process as illustrated in Fig. 9b (Skourtis et al. 2016), which is a double electron exchange between the photoexcited fluorophore and a partially filled d-orbital of appropriate energy. An electron is transferred from the donor side to an acceptor molecule in quenching process via wave function overlapping that which requires a very short distance (< 10 Å). When multiple metal ions are simultaneously involved in this sensing process, then there is a challenge of distinguishing a particular type of metal ions and it complicates the "turn on" sensors. Transition metal ions such as Cu^{2+}, Fe^{3+} with their vacant low-lying d-orbitals (acceptor) can bind to the electron rich Cb-QDs (donor) by complexing with the $–COO^-$ groups present on the surface. The electron transfer from electron-rich Cb-QDs to metal ions in the excited state quenches the fluorescence signaling resulting in a reduction of PL intensity ("ON–OFF" process). The time-correlated single photon counting (TCSPC) can measure the lifespan of Cb-QDs and the metal – Cb-QDs complex, which indicates that if the lifespan decreases

Table 4 SWs-derived Cb-QDs for environmental and catalytic applications

Raw material	Environmental application	Limit of detection (LOD)	Reference
CQDs			
Carboxymethyl cellulose	Sensor to detect Cu^{2+} in real water	0.93 µM	(Abdullah Issa et al. 2019)
Orange peels	Sensor to detect Fe^{3+}	0.073 µM	(Wang et al. 2020)
Banana pseudo-stem	Detection of Fe^{3+} ion	6.4 nM	(Vandarkuzhali et al. 2017)
Vehicle exhaust soot	Sensor to detect tetrazine in soft drinks	26 nM	(Thulasi et al. 2020)
Bagasse waste	Sensor to detect Hg^{2+} ions	0.002 µM	(Xu-Cheng et al. 2018)
Papaya waste pulp	Level free chemo probe for Cr^{6+} detection in water	0.708 µg/L	(D. et al. 2019)
Petroleum coke	Cu^{2+} ion detection	0.0295 µM	(Wang et al. 2015a)
Kerosene soot	Detection of picric acid, Fe^{3+} and Cu^{2+} ions	PA = 86 ng/mL Cu^{2+} = 15.3 ng/mL Fe^{3+} = 0.36 µg/mL	(Venkatesan et al. 2019)
Cat feedstock waste	Fe^{3+} ion detection	32 µM	(Ahn et al. 2019)
Waste carbon paper	Probe for trinitrotoluene detection	7.4 µg/L	(Devi et al. 2018)
Whey	Sensors for selenite in water	0.035 µg/L	(Devi et al. 2017)
Expired milk	Sensor for detection of Fe^{3+} ions and fluorescent patterning	-	(Su et al. 2018)
Expired milk	Sensors for Cr^{6+} ions	14 µM	(Athika et al. 2019)
Goose feather	Detection of Fe^{3+} ions	196 nM	(Liu et al. 2015)
Pigeon feather, egg, and manure	Detection of Fe^{3+} and Hg^{2+} ions	Fe^{3+} = 60.9 nM Hg^{2+} = 10.3 nM	(Ye et al. 2017)
Prawn shell	Detection of Cu^{2+} ions (also sea water samples)	5 nM	(Gedda et al. 2016)
Palm kernel shell	Detection and removal of Cu^{2+} ions	-	(Ang et al. 2020)
Orange peel	Detection of *E. coli* in milk	487 CFU/mL	(Hu et al. 2021)
Lemon peel	Detection of Cr^{6+} ions	73 nM	(Tyagi et al. 2016)
Wheat straw	Detection of Fe^{3+} ion	1.95 µM	(Yuan et al. 2015)
Wheat straw	Detection of F^-	49 µM	(Liu et al. 2021b)
Tea waste	Detection of CrO_4^{2-}, Fe^{3+}, ascorbic acid, L-cysteine in real samples	CrO_4^{2-} = 0.81 µM Fe^{3+} = 0.15 µM Ascorbic acid = 19.78 µM (by CQDs-limit Fe^{3+} system) and 87.02 µM (by CQDs-CrO_4^{2-} system) L-cysteine = 153.5 µM (by CQDs-Fe^{3+} system) and 8.785 µM (by CQDs-CrO_4^{2-} system)	(Chen et al. 2019)
Egg shell membrane	Detection of GSH	0.48 µM	(Wang et al. 2012)
Egg shell membrane	Determination of Hg^{2+} ions	2.6 µM	(Ye et al. 2020)
Human hair	Chloroform sensing in water	3 µg/L	(Singh et al. 2020)
Human hair	Hg^{2+} ion detection	10 nM	(Guo et al. 2016)
Orange peels	Photocatalytic degradation of naphthol blue-black (azo dye)	-	(Prasannan and Imae 2013)
Lemon peel	Photocatalytic degradation of Methylene blue	-	(Tyagi et al. 2016)
GQDs			
Spent tea waste	Sensor to detect Fe^{3+}	2.5 ± 0.3 µM	(Abbas et al. 2020)
Dead neem leaves	On–off-on probe for Ag^+ ions	0.033–0.1 g/L	(Suryawanshi et al. 2014)

significantly, then there must be the electron transfer on that complex (Wang et al. 2015a). When another strong chelating compound (ligand) is introduced to the metal ion – Cb-QDs complex solution, it triggers a chelation competition and, as a result, separates the "alien" metal ions by chelation. Thus, the fluorescent activity is regained ("OFF–ON" part). A description of "ON–OFF-ON" pathway is given in Fig. 9e. The total process is supported by Dexter energy transfer mechanism.

While sensing organic molecules including DNA and TNT, π* (antibonding orbital) of the acceptor molecule is involved (Demchenko and Dekaliuk 2013) in the reduction of PL intensity and causes the turn- "OFF" the fluorescent signal. Now if another molecule possing strong binding efficiency with that organic molecule added to that organic molecule – Cb-QDs complex solution, then the fluorescence signal (turn- "ON") will be restored. Thus, as electron deficiency or electron accepting inclination increases, electron transfer from donor Cb-QDs to metal ions/organic molecules increases, resulting in a greater reduction of PL intensity. As a result, increase in sensitivity occurs with a significant increase in LOD efficiency.

The second mechanism is photoinduced electron transfer, or PET, which includes charge separation and excitation of the donor side via irradiation (Jose et al. 2017), resulting in either fluorescence quenching or amplification. Here, the electron transfer between the metal ion and the fluorophore, or inside the self-fluorophore-chelate unit, can also result in fluorescence property modulation (Fig. 9c). Direct electronic transitions between fluorophores (excited) and metal ions, containing low energy d-orbitals (empty or partially filled) are usually accompanied by quenching. PET can also enhance the fluorescence for fluorophore-electron rich metal chelate. Without metal ions, excitation leads to the separation of charges, and hence, the PET in between excited fluorophore and chelate goes in for emission, thereby PET gives rise to systematic relaxation pathway and resulting a decrease in QY for that fluorophore. When a metal ion binds to an electron-rich chelating site, a shifting of charge density occurs and thus effectively quenches the PET decay pathway, resulting in the increase in QY.

Another mechanism that involves radiation-free energy transfer through dipole–dipole coupling between a photoexcited donor and an acceptor is known as Forster resonance energy transfer, FRET (Masters 2014) (Fig. 9d). FRET efficiency of energy transfer is highly dependent on the distance (inversely and to the sixth power) between the donor and acceptor. The acceptor can be a chromophore (capable of absorbing energy) or a fluorophore, in which a photon is irradiated by a high energy molecule during relaxation to the low energy state due to sensitized emission. In general, FRET reduces donor emissions, resulting in a shorter lifetime. Metal binding results in a change in molecule structure and can affect distance and/or orientation that can assist or hinder FRET (Carter et al. 2014).

The mechanism for the fluorescence emission is still ambiguous due to the different theories among the researchers. The bioimaging within the cells are primarily due to the fluorescence emission property of CQDs. In general, two mechanisms are widely accepted for CQDs: excitation dependent and excitation independent. The excitation dependent fluorescence is primarily due to band gap emissions in π-domain where strong absorption in the UV range and a weak emission is observed. Surface defects in the structure of CQDs induce excitation independent fluorescence emission, which exhibits mild absorption and high emission in the visible region.

Defects in GQDs containing sp^3 carbons are structurally comparable to those observed on the surface of tiny CQDs with an unusually high surface-to-volume ratio (Cao et al. 2013). According to Molaei group, the PL mechanism observed in GQDs is primarily due to surface defects and band gap transitions associated with conjugated π -domains (Molaei 2019). It is possible to use GQDs with near infrared (NIR) emission for bioimaging because tissues often exhibit autofluorescence and low light absorption in the NIR region (Younis et al. 2020).

Comparison of CQDs, GQDs, and GOQDs based on their synthesis, structures, physical properties, and chemical properties

The summary of SW-based Cb-QDs in terms of synthesis, structures as well as their physical and chemical properties are given in Table 5. It is evident that CQDs do not demonstrate any selectivity in their synthesis, but the structure of SWs plays a significant role during the synthesis of both GQDs and GOQDs. Though the surface functionalities of GOQDs are more compared to CQDs and GQDs, yet it is less explored because of its low fluorescent intensity than other two QDs.

Table 5 Comparison of SWs-derived CQDs, GQDs, and GOQDs based on their synthesis, structures, physical properties, and chemical properties

Properties	CQDs	GQDs	GOQDs
Synthesis	Can be synthesized from almost any source with high carbon ratio	Top down approach requires specific carbon skeleton of starting materials, like benzene, naphthalene ring	Top down approach requires specific carbon skeleton of starting materials, like benzene, naphthalene ring
Structure	Spherical structure	Sheet-like structure	Sheet-like structure
Carbon/Oxygen ratio	More	More	Less
Polarity	Less polar and water soluble	Less polar and water soluble	More polar, more water soluble
Surface functionalities	Less	Less	More
Fluorescent intensity	More	More	Less

Limitations and future research prospects of carbon-based quantum dots

Cb-QDs have been employed as a selective or non-selective medication, gene, and drug delivery agent for in vivo or in vitro studies on a certain kind of cell. Because of their stable PL, these materials are highly suitable for sensing in vivo and in vitro cells. Aside from medicinal uses, these materials are also employed for energy storage or batteries, as well as for the detection of toxic elements, ions or molecules, and explosives due to their high fluorescence and low and adjustable band gap.

Apart from these, there are many other applications of Cb-QDs. Lu et al. (2015) reported better photocatalytic activity of zinc-porphyrin modified GQDs compared to zinc-porphyrin towards the degradation of methylene blue (MB) under visible-light. On the other hand, Dang et al. (2022) used Fe-doped CQDs to generate methanol by CO_2 reduction. A three-fold increase in photocatalytic activity of S and N co-doped CQDs with TiO_2 NPs was observed towards acid red 88 degradation (Rahbar et al. 2019). Tammina et al. (2019) reported the application of N and P co-doped CQDs as dopamine sensor with a detection limit of 0.021 M. In another study, the use of N-doped GQDs, as a sensor, was reported for the detection of Fe^{3+} with high selectivity and sensitivity (Tam et al. 2014). Malček et al. (2022), through theoretical modelling, reported that Mn and Cr doped GQDs were highly effective at adsorbing H_2 gas.

The fuel cell applications of doped CQDs and GQDs were also reported. N-doped CQDs decorated on the carbon paper surface were used to develop microbial fuel cell anode (Shaari et al. 2021). According to Yun et al. (2019), the composite materials made of porous Fe_2O_3, nitrogen-doped CQDs, and reduced graphene oxide make good electrode materials for alkaline aqueous batteries.

Mahat et al. (2020) proposed green synthesis of palm oil biomass-based CQDs- embedded into polysulfone-selective layers to develop thin-film composite membranes for forward osmosis. To get highly selective water transport for high-performance nanofiltration via interfacial polymerization, Lin et al. (2021) synthesized a unique class of thin-film composite nanofiltration membranes that were directly formed from assembled GQDs with amino/sulfonic alteration. For the quantitative determination of Ce^{4+} from aqueous solution, Chu et al. (2020) synthesized N-doped GQDs from GO with a detection limit of 0.8352 M and higher selectivity compared to other rare earth elements.

Even though, Cb-QDs have been well developed, they are still restricted to research laboratories, and only a few applications for use in the real world have been developed. Due to the lack of a simple and large-scale production technology for preparing Cb-QDs, realistic application level is almost untouched in the present scenario. To broaden the commercialization possibilities of Cb-QDs in the future, research into the synthesis of these QDs with desired forms, sizes, and targeting regions with perfectly adjusted surfaces and well-tuned band gaps needs to be conducted. The biggest concern among researchers working on Cb-QDs for various nanomedical, environmental, and energy-related applications is increasing the conversion yields. The existing synthetic processes only allow for the small-scale manufacture of Cb-QDs with a broad size distribution. In most of the reported synthetic procedures, the unreacted starting materials are not conveniently removed. Therefore, improved methods for purifying synthesized QDs are a need of an hour. Cb-QDs will undoubtedly be beneficial in more innovative applications because of their outstanding PL, uniform size distribution, and high QYs.

Cb-QDs are yet to be regarded as safe materials, therefore, more advanced research is needed to achieve their pure and non-toxicological form. Aside from toxicity, another issue is that the existing process does not produce high-quality products and, as a result, they cannot be used in nanomedicine at this time. Although Cb-QDs have been used with and without surface modifications, their selectivity for the absorption of certain toxic/radioactive elements/ions/molecules remains low. More specific mechanisms related to the adjustment of PL features must be explored, whereas a few likely processes, such as doping, size effect, and surface functionalization, have been found. The physical and chemical characteristics of Cb-QDs are yet to be clearly described. Cb-QDs research for gene delivery is still in its early phase, therefore more focus is required in this area. Moreover, due to their outstanding sensing capabilities, Cb-QDs could be effectively exploited in COVID-19.

Keeping in mind the potential of surface functionalized Cb-QDs in the near future, we have a strong ly believe that more sophisticated and innovative research will be developed on the advancement of re-functionalization methods to get rid of disadvantages relating to the Cb-QDs for physical, chemical, and biological applications. After improving the properties of Cb-QDs, e.g., size, PL, and band gap, they can be used as better storage of energy, good catalyst, better delivery agents and imaging and sensing probes. SWs sources provide Cb-QDs with very poor product yield and QY, especially when GQDs and GOQDs are synthesized. As a result, the application portion for the linked waste products is not widespread. Apart from the wide range of applications of Cb-QDs, there are still a lot of hurdles that are needed to overcome different drawbacks.

Conclusions

SW-derived Cb-QDs are inexpensive, reducing the cost of imaging, sensing, and detection applications. Carbon enriched SWs are the best raw materials for the production

of Cb-QDs while agricultural and food wastes are topping up the list. Among the SWs-derived Cb-QDs, CQDs are the best QDs, as they can be produced with higher QY than the GQDs and GOQDs. Hence, SWs can be utilized in the form of CQDs with versatile applicability. Because of the low QY associated with them, to date, GQDs and GOQDs have not had broad utility. As of now, Cb-QDs are not very popular materials for practical applications because of their poor reproducibility during large scale synthesis. Therefore, a lot of opportunities are still there for future researchers to develop advanced pathways for their synthesis and applications. There is also a potential for converting tons of SWs generated daily in rural and urban areas into environmentally benign Cb-QDs for more practical utilization.

Author contribution Chanchal Das: conceptualization, methodology, data curation, and writing—original draft. Mika Sillanpää: writing—reviewing and editing. Shabi Abbas Zaidi: writing—reviewing and editing. Moonis Ali Khan: conceptualization, methodology, and writing—reviewing and editing. Goutam Biswas: conceptualization, methodology, validation, and writing—reviewing and editing.

Funding Chanchal Das and Goutam Biswas received grants from the Department of Chemistry, Cooch Behar Panchanan Barma University.

Declarations

Ethical approval Not applicable.

Consent to participate Not applicable.

Consent for publication Not applicable.

Competing interests The authors declare no competing interests.

References

Abbas A, Tabish TA, Bull SJ, Lim TM, Phan AN (2020) High yield synthesis of graphene quantum dots from biomass waste as a highly selective probe for Fe^{3+} sensing. Sci Rep 10:21262. https://doi.org/10.1038/s41598-020-78070-2

Abdel-Shafy HI, Mansour MSM (2018) Solid waste issue: sources, composition, disposal, recycling, and valorization. Egypt J Pet 27:1275–1290. https://doi.org/10.1016/j.ejpe.2018.07.003

Abdullah Issa MZ, Abidin Z, Sobri S, Rashid S, Adzir Mahdi M, Azowa Ibrahim N, Pudza YM (2019) Facile synthesis of nitrogen-doped carbon dots from lignocellulosic waste. Nanomaterials 9:1500. https://doi.org/10.3390/nano9101500

Adebayo (2011) Spectrophotometric determination of iron (III) in tap water using 8-hydoxyquinoline as a chromogenic reagent. AFRICAN J Biotechnol 10(16051):16057. https://doi.org/10.5897/AJB10.1840

Adolfsson KH, Hassanzadeh S, Hakkarainen M (2015) Valorization of cellulose and waste paper to graphene oxide quantum dots. RSC Adv 5:26550–26558. https://doi.org/10.1039/C5RA01805F

Ahirwar S, Mallick S, Bahadur D (2017) Electrochemical method to prepare graphene quantum dots and graphene oxide quantum dots. ACS Omega 2:8343–8353. https://doi.org/10.1021/acsomega.7b01539

Ahn J, Song Y, Kwon JE, Lee SH, Park KS, Kim S, Woo J, Kim H (2019) Food waste-driven N-doped carbon dots: applications for Fe^{3+} sensing and cell imaging. Mater Sci Eng C 102:106–112. https://doi.org/10.1016/j.msec.2019.04.019

Al Jahdaly BA, Elsadek MF, Ahmed BM, Farahat MF, Taher MM, Khalil AM (2021) Outstanding graphene quantum dots from carbon source for biomedical and corrosion inhibition applications: a review. Sustainability 13:2127. https://doi.org/10.3390/su13042127

Alaghmandfard A, Sedighi O, TabatabaeiRezaei N, Abedini AA, MalekKhachatourian A, Toprak MS, Seifalian A (2021) Recent advances in the modification of carbon-based quantum dots for biomedical applications. Mater Sci Eng C 120:111756. https://doi.org/10.1016/j.msec.2020.111756

Algar WR, Massey M, Rees K, Higgins R, Krause KD, Darwish GH, Peveler WJ, Xiao Z, Tsai H-Y, Gupta R, Lix K, Tran MV, Kim H (2021) Photoluminescent nanoparticles for chemical and biological analysis and imaging. Chem Rev 121:9243–9358. https://doi.org/10.1021/acs.chemrev.0c01176

Alkian I, Sutanto H, Hadiyanto, (2022) Quantum yield optimization of carbon dots using response surface methodology and its application as control of Fe^{3+} ion levels in drinking water. Mater Res Express 9:015702. https://doi.org/10.1088/2053-1591/ac3f60

Alvand ZM, Rajabi HR, Mirzaei A, Sajadiasl F (2021) Combination of plant-mediated and sonochemical-assisted synthesis for preparation of low-toxic cadmium selenide semiconductor nanoparticles: study of the effect of extraction techniques, characterization, comparative study of biological activities. Surf Interfaces 25:101182. https://doi.org/10.1016/j.surfin.2021.101182

Ang WL, Boon Mee CAL, Sambudi NS, Mohammad AW, Leo CP, Mahmoudi E, Ba-Abbad M, Benamor A (2020) Microwave-assisted conversion of palm kernel shell biomass waste to photoluminescent carbon dots. Sci Rep 10:21199. https://doi.org/10.1038/s41598-020-78322-1

Anthony AM, Murugan R, Subramanian R, Selvarangan GK, Pandurangan P, Dhanasekaran A, Sohrab A (2020) Ultra-radiant photoluminescence of glutathione rigidified reduced carbon quantum dots (r-CQDs) derived from ice-biryani for in vitro and in vivo bioimaging applications. Colloids Surfaces A Physicochem Eng Asp 586:124266. https://doi.org/10.1016/j.colsurfa.2019.124266

Arias Velasco V, Caicedo Chacón WD, Carvajal Soto AM, Ayala Valencia G, Granada Echeverri JC, Agudelo Henao AC (2021) Carbon quantum dots based on carbohydrates as nano sensors for food quality and safety. Starch - Stärke 73:2100044. https://doi.org/10.1002/star.202100044

Atchudan R, Edison TNJI, Perumal S, Vinodh R, Sundramoorthy AK, Babu RS, Lee YR (2021) Leftover kiwi fruit peel-derived carbon dots as a highly selective fluorescent sensor for detection of ferric ion. Chemosensors 9:166. https://doi.org/10.3390/chemosensors9070166

Athika M, Prasath A, Duraisamy E, Sankar Devi V, Selva Sharma A, Elumalai P (2019) Carbon-quantum dots derived from denatured milk for efficient chromium-ion sensing and supercapacitor applications. Mater Lett 241:156–159. https://doi.org/10.1016/j.matlet.2019.01.064

Bagheri Z, Ehtesabi H, Hallaji Z, Latifi H, Behroodi E (2018) Investigation the cytotoxicity and photo-induced toxicity of carbon dot on yeast cell. Ecotoxicol Environ Saf 161:245–250. https://doi.org/10.1016/j.ecoenv.2018.05.071

Bankoti K, Rameshbabu AP, Datta S, Das B, Mitra A, Dhara S (2017) Onion derived carbon nanodots for live cell imaging and accelerated skin wound healing. J Mater Chem B 5:6579–6592. https://doi.org/10.1039/C7TB00869D

Baweja H, Jeet K (2019) Economical and green synthesis of graphene and carbon quantum dots from agricultural waste. Mater Res Express 6:0850g8. https://doi.org/10.1088/2053-1591/ab28e5

Bruno F, Sciortino A, Buscarino G, Soriano ML, Ríos Á, Cannas M, Gelardi F, Messina F, Agnello S (2021) A comparative study of top-down and bottom-up carbon nanodots and their interaction with mercury ions. Nanomaterials 11:1265. https://doi.org/10.3390/nano11051265

Bui T-D, Tseng J-W, Tseng M-L, Lim MK (2022) Opportunities and challenges for solid waste reuse and recycling in emerging economies: a hybrid analysis. Resour Conserv Recycl 177:105968. https://doi.org/10.1016/j.resconrec.2021.105968

Buzaglo M, Shtein M, Regev O (2016) Graphene quantum dots produced by microfluidization. Chem Mater 28:21–24. https://doi.org/10.1021/acs.chemmater.5b03301

Cao L, Meziani MJ, Sahu S, Sun Y-P (2013) Photoluminescence properties of graphene versus other carbon nanomaterials. Acc Chem Res 46:171–180. https://doi.org/10.1021/ar300128j

Carter KP, Young AM, Palmer AE (2014) Fluorescent sensors for measuring metal ions in living systems. Chem Rev 114:4564–4601. https://doi.org/10.1021/cr400546e

Chen F, Gao W, Qiu X, Zhang H, Liu L, Liao P, Fu W, Luo Y (2017) Graphene quantum dots in biomedical applications: recent advances and future challenges. Front Lab Med 1:192–199. https://doi.org/10.1016/j.flm.2017.12.006

Chen K, Qing W, Hu W, Lu M, Wang Y, Liu X (2019) On-off-on fluorescent carbon dots from waste tea: their properties, antioxidant and selective detection of CrO_4^{2-}, Fe^{3+}, ascorbic acid and L-cysteine in real samples. Spectrochim. Acta Part A Mol Biomol Spectrosc 213:228–234. https://doi.org/10.1016/j.saa.2019.01.066

Chen BB, Liu ML, Huang CZ (2020) Carbon dot-based composites for catalytic applications. Green Chem 22:4034–4054. https://doi.org/10.1039/D0GC01014F

Cheng C, Shi Y, Li M, Xing M, Wu Q (2017) Carbon quantum dots from carbonized walnut shells: structural evolution, fluorescence characteristics, and intracellular bioimaging. Mater Sci Eng C 79:473–480. https://doi.org/10.1016/j.msec.2017.05.094

Chien C-F, Aviso K, Tseng M-L, Fujii M, Lim MK (2021) Solid waste management in emerging economies: opportunities and challenges for reuse and recycling. Resour Conserv Recycl 172:105677. https://doi.org/10.1016/j.resconrec.2021.105677

Chiu S-H, Gedda G, Girma WM, Chen J-K, Ling Y-C, Ghule AV, Ou K-L, Chang J-Y (2016) Rapid fabrication of carbon quantum dots as multifunctional nanovehicles for dual-modal targeted imaging and chemotherapy. Acta Biomater 46:151–164. https://doi.org/10.1016/j.actbio.2016.09.027

Chromium in Drinking Water | US EPA [WWW Document] (n.d.) URL https://www.epa.gov/sdwa/chromium-drinking-water (accessed 1.9.22)

Chu X, Wang S, Cao Y (2020) A new fluorescence probe comprising nitrogen-doped graphene quantum dots for the selective and quantitative determination of cerium(iv). New J Chem 44:797–806. https://doi.org/10.1039/C9NJ04518J

Cunci L, González-Colón V, Lee Vargas-Pérez B, Ortiz-Santiago J, Pagán M, Carrion P, Cruz J, Molina-Ontoria A, Martinez N, Silva W, Echegoyen L, Cabrera CR (2021) Multicolor fluorescent graphene oxide quantum dots for sensing cancer cell biomarkers. ACS Appl Nano Mater 4:211–219. https://doi.org/10.1021/acsanm.0c02526

D'Angelis do E. S. Barbosa C, Corrêa JR, Medeiros GA, Barreto G, Magalhães KG, de Oliveira AL, Spencer J, Rodrigues MO, Neto BAD (2015) Carbon dots (C-dots) from cow manure with impressive subcellular selectivity tuned by simple chemical modification. Chem-A Eur J 21:5055–5060. https://doi.org/10.1002/chem.201406330

D'souza SL, Chettiar SS, Koduru JR, Kailasa SK (2018) Synthesis of fluorescent carbon dots using Daucus carota subsp. sativus roots for mitomycin drug delivery. Optik (stuttg) 158:893–900. https://doi.org/10.1016/j.ijleo.2017.12.200

Dalal C, Saini D, Garg AK, Sonkar SK (2021) Fluorescent carbon nano-onion as bioimaging probe. ACS Appl Bio Mater 4:252–266. https://doi.org/10.1021/acsabm.0c01192

Dang Y, Li B, Feng X, Jia J, Li K, Zhang Y (2022) Preparation of iron-doped carbon dots and their application in photocatalytic reduction of carbon dioxide. ChemPhotoChem. https://doi.org/10.1002/cptc.202200156

Das R, Bandyopadhyay R, Pramanik P (2018) Carbon quantum dots from natural resource: a review. Mater Today Chem 8:96–109. https://doi.org/10.1016/j.mtchem.2018.03.003

Das C, Paul SS, Saha A, Singh T, Saha A, Im J, Biswas G (2020) Silver-based nanomaterials as therapeutic agents against coronaviruses: a review. Int J Nanomedicine 15:9301–9315. https://doi.org/10.2147/IJN.S280976

Das C, Singh S, Bhakta S, Mishra P, Biswas G (2022) Bio-modified magnetic nanoparticles with Terminalia arjuna bark extract for the removal of methylene blue and lead (II) from simulated wastewater. Chemosphere 291:132673. https://doi.org/10.1016/j.chemosphere.2021.132673

David K, Pu Y, Foston M, Muzzy J, Ragauskas A (2009) Cross-polarization/magic angle spinning (CP/MAS) ^{13}C nuclear magnetic resonance (NMR) analysis of chars from alkaline-treated pyrolyzed softwood. Energy Fuels 23:498–501. https://doi.org/10.1021/ef8004527

de Boëver R, Town JR, Li X, Claverie JP (2022) Carbon dots for carbon dummies: the quantum and the molecular questions among some others. Chem–A Eur J 28:e202200748. https://doi.org/10.1002/chem.202200748

Demchenko AP, Dekaliuk MO (2013) Novel fluorescent carbonic nanomaterials for sensing and imaging. Methods Appl Fluoresc 1:042001. https://doi.org/10.1088/2050-6120/1/4/042001

Desmond LJ, Phan AN, Gentile P (2021) Critical overview on the green synthesis of carbon quantum dots and their application for cancer therapy. Environ Sci Nano 8:848–862. https://doi.org/10.1039/D1EN00017A

Devi P, Kaur G, Thakur A, Kaur N, Grewal A, Kumar P (2017) Waste derivitized blue luminescent carbon quantum dots for selenite sensing in water. Talanta 170:49–55. https://doi.org/10.1016/j.talanta.2017.03.069

Devi S, Gupta RK, Paul AK, Tyagi S (2018) Waste carbon paper derivatized carbon quantum dots/(3-Aminopropyl)triethoxysilane based fluorescent probe for trinitrotoluene detection. Mater. Res. Express 6:025605. https://doi.org/10.1088/2053-1591/aaf03c

Ding Z, Li F, Wen J, Wang X, Sun R (2018) Gram-scale synthesis of single-crystalline graphene quantum dots derived from lignin biomass. Green Chem 20:1383–1390. https://doi.org/10.1039/C7GC03218H

Dong Y, Shao J, Chen C, Li H, Wang R, Chi Y, Lin X, Chen G (2012) Blue luminescent graphene quantum dots and graphene oxide prepared by tuning the carbonization degree of citric acid. Carbon n y 50:4738–4743. https://doi.org/10.1016/j.carbon.2012.06.002

Facure MHM, Schneider R, Mercante LA, Correa DS (2020) A review on graphene quantum dots and their nanocomposites: from laboratory synthesis towards agricultural and environmental applications. Environ Sci Nano 7:3710–3734. https://doi.org/10.1039/D0EN00787K

Fakhraie S, Rajabi HR, Rashidi A (2023) Fabrication and application of novel core–shell MIL-101(Cr)@UiO-66(Zr) nanocrystals for highly selective separation of H_2S and CO_2. Chem Eng J 452:139001. https://doi.org/10.1016/j.cej.2022.139001

Gao L, Li R, Sui X, Li R, Chen C, Chen Q (2014) Conversion of chicken feather waste to N-doped carbon nanotubes for the catalytic reduction of 4-nitrophenol. Environ Sci Technol 48:10191–10197. https://doi.org/10.1021/es5021839

Gedda G, Lee C-Y, Lin Y-C, Wu H (2016) Green synthesis of carbon dots from prawn shells for highly selective and sensitive detection of copper ions. Sensors Actuators B Chem 224:396–403. https://doi.org/10.1016/j.snb.2015.09.065

Gomes MF, Gomes YF, Lopes-Moriyama A, de Barros Neto EL, de Souza CP (2019) Design of carbon quantum dots via hydrothermal carbonization synthesis from renewable precursors. Biomass Convers Biorefinery 9:689–694. https://doi.org/10.1007/s13399-019-00387-4

Guo Y, Zhang L, Cao F, Leng Y (2016) Thermal treatment of hair for the synthesis of sustainable carbon quantum dots and the applications for sensing Hg^{2+}. Sci Rep 6:35795. https://doi.org/10.1038/srep35795

Halder A, Godoy-Gallardo M, Ashley J, Feng X, Zhou T, Hosta-Rigau L, Sun Y (2018) One-pot green synthesis of biocompatible graphene quantum dots and their cell uptake studies. ACS Appl Bio Mater 1:452–461. https://doi.org/10.1021/acsabm.8b00170

Horst FH, da Silva Rodrigues CV, Carvalho PHPR, Leite AM, Azevedo RB, Neto BAD, Corrêa JR, Garcia MP, Alotaibi S, Henini M, Chaves SB, Rodrigues MO (2021) From cow manure to bioactive carbon dots: a light-up probe for bioimaging investigations, glucose detection and potential immunotherapy agent for melanoma skin cancer. RSC Adv 11:6346–6352. https://doi.org/10.1039/D0RA10859F

Hu L, Sun Y, Li S, Wang X, Hu K, Wang L, Liang X, Wu Y (2014a) Multifunctional carbon dots with high quantum yield for imaging and gene delivery. Carbon n y 67:508–513. https://doi.org/10.1016/j.carbon.2013.10.023

Hu Y, Yang J, Tian J, Jia L, Yu J-S (2014b) Waste frying oil as a precursor for one-step synthesis of sulfur-doped carbon dots with pH-sensitive photoluminescence. Carbon n y 77:775–782. https://doi.org/10.1016/j.carbon.2014.05.081

Hu C, Su T-R, Lin T-J, Chang C-W, Tung K-L (2018) Yellowish and blue luminescent graphene oxide quantum dots prepared via a microwave-assisted hydrothermal route using H 2 O 2 and KMnO 4 as oxidizing agents. New J Chem 42:3999–4007. https://doi.org/10.1039/C7NJ03337K

Hu X, Li Yanxiao, Xu Y, Gan Z, Zou X, Shi J, Huang X, Li Z, Li Yahui (2021) Green one-step synthesis of carbon quantum dots from orange peel for fluorescent detection of Escherichia coli in milk. Food Chem 339:127775. https://doi.org/10.1016/j.foodchem.2020.127775

Huang C, Li X, Tung C, Wu L (2018) Photocatalysis with quantum dots and visible light for effective organic synthesis. Chem–A Eur J 24:11530–11534. https://doi.org/10.1002/chem.201800391

Jeong Y, Moon K, Jeong S, Koh W-G, Lee K (2018) Converting waste papers to fluorescent carbon dots in the recycling process without loss of ionic liquids and bioimaging applications. ACS Sustain Chem Eng 6:4510–4515. https://doi.org/10.1021/acssuschemeng.8b00353

Jose AR, Vikraman AE, Girish Kumar K (2017) Photoinduced electron transfer between quantum dots and pralidoxime: an efficient sensing strategy. New J Chem 41:10828–10834. https://doi.org/10.1039/C7NJ00795G

Kang S, Kim KM, Jung K, Son Y, Mhin S, Ryu JH, Shim KB, Lee B, Han H, Song T (2019) Graphene oxide quantum dots derived from coal for bioimaging: facile and green approach. Sci Rep 9:4101. https://doi.org/10.1038/s41598-018-37479-6

Khan WU, Wang D, Zhang W, Tang Z, Ma X, Ding X, Du S, Wang Y (2017) High quantum yield green-emitting carbon dots for Fe(III) detection, biocompatible fluorescent ink and cellular imaging. Sci Rep 7:14866. https://doi.org/10.1038/s41598-017-15054-9

Khan AH, López-Maldonado EA, Khan NA, Villarreal-Gómez LJ, Munshi FM, Alsabhan AH, Perveen K (2021) Current solid waste management strategies and energy recovery in developing countrihes - state of art review. Chemosphere 291:133088. https://doi.org/10.1016/j.chemosphere.2021.133088

Khan S, Anjum R, Raza ST, Ahmed Bazai N, Ihtisham M (2022) Technologies for municipal solid waste management: current status, challenges, and future perspectives. Chemosphere 288:132403. https://doi.org/10.1016/j.chemosphere.2021.132403

Kim D, Yoo JM, Hwang H, Lee J, Lee SH, Yun SP, Park MJ, Lee M, Choi S, Kwon SH, Lee Saebom, Kwon S-H, Kim S, Park YJ, Kinoshita M, Lee Y-H, Shin S, Paik SR, Lee SJ, Lee S, Hong BH, Ko HS (2018) Graphene quantum dots prevent α-synucleinopathy in Parkinson's disease. Nat Nanotechnol 13:812–818. https://doi.org/10.1038/s41565-018-0179-y

Kolahalam LA, Kasi Viswanath IV, Diwakar BS, Govindh B, Reddy V, Murthy YLN (2019) Review on nanomaterials: synthesis and applications. Mater Today Proc 18:2182–2190. https://doi.org/10.1016/j.matpr.2019.07.371

Kumar R, Kumar VB, Gedanken A (2020a) Sonochemical synthesis of carbon dots, mechanism, effect of parameters, and catalytic, energy, biomedical and tissue engineering applications. Ultrason Sonochem 64:105009. https://doi.org/10.1016/j.ultsonch.2020.105009

Kumar YR, Deshmukh K, Sadasivuni KK, Pasha SKK (2020b) Graphene quantum dot based materials for sensing, bio-imaging and energy storage applications: a review. RSC Adv 10:23861–23898. https://doi.org/10.1039/D0RA03938A

Kusic H, Leszczynska D, Koprivanac N, Peternel I (2011) Role of quantum dots nanoparticles in the chemical treatment of colored wastewater: catalysts or additional pollutants. J Environ Sci 23:1479–1485. https://doi.org/10.1016/S1001-0742(10)60609-2

Lettieri S, Camisasca A, D'Amora M, Diaspro A, Uchida T, Nakajima Y, Yanagisawa K, Maekawa T, Giordani S (2017a) Far-red fluorescent carbon nano-onions as a biocompatible platform for cellular imaging. RSC Adv 7:45676–45681. https://doi.org/10.1039/C7RA09442F

Lettieri S, D'Amora M, Camisasca A, Diaspro A, Giordani S (2017b) Carbon nano-onions as fluorescent on/off modulated nanoprobes for diagnostics. Beilstein J Nanotechnol 8:1878–1888. https://doi.org/10.3762/bjnano.8.188

Li C, Shi G (2014) Carbon nanotube-based fluorescence sensors. J Photochem Photobiol C Photochem Rev 19:20–34. https://doi.org/10.1016/j.jphotochemrev.2013.10.005

Li M, Chen T, Gooding JJ, Liu J (2019) Review of carbon and graphene quantum dots for sensing. ACS Sensors 4:1732–1748. https://doi.org/10.1021/acssensors.9b00514

Lin Y, Shen Q, Kawabata Y, Segawa J, Cao X, Guan K, Istirokhatun T, Yoshioka T, Matsuyama H (2021) Graphene quantum dots (GQDs)-assembled membranes with intrinsic functionalized nanochannels for high-performance nanofiltration. Chem Eng J 420:127602. https://doi.org/10.1016/j.cej.2020.127602

Liu S-S, Wang C-F, Li C-X, Wang J, Mao L-H, Chen S (2014) Hair-derived carbon dots toward versatile multidimensional fluorescent materials. J Mater Chem C 2:6477–6483. https://doi.org/10.1039/C4TC00636D

Liu R, Zhang J, Gao M, Li Z, Chen J, Wu D, Liu P (2015) A facile microwave-hydrothermal approach towards highly photoluminescent carbon dots from goose feathers. RSC Adv 5:4428–4433. https://doi.org/10.1039/C4RA12077A

Liu M, Xu Y, Niu F, Gooding JJ, Liu J (2016) Carbon quantum dots directly generated from electrochemical oxidation of graphite electrodes in alkaline alcohols and the applications for specific

ferric ion detection and cell imaging. Analyst 141:2657–2664. https://doi.org/10.1039/C5AN02231B

Liu X, Xu T, Li Y, Zang Z, Peng X, Wei H, Zha W, Wang F (2018) Enhanced X-ray photon response in solution-synthesized $CsPbBr_3$ nanoparticles wrapped by reduced graphene oxide. Sol Energy Mater Sol Cells 187:249–254. https://doi.org/10.1016/j.solmat.2018.08.009

Liu J, Li R, Yang B (2020) Carbon dots: a new type of carbon-based nanomaterial with wide applications. ACS Cent Sci 6:2179–2195. https://doi.org/10.1021/acscentsci.0c01306

Liu S, Liu Z, Li Q, Xia H, Yang W, Wang R, Li Y, Zhao H, Tian B (2021a) Facile synthesis of carbon dots from wheat straw for colorimetric and fluorescent detection of fluoride and cellular imaging. Spectrochim Acta Part A Mol Biomol Spectrosc 246:118964. https://doi.org/10.1016/j.saa.2020.118964

Liu Y-Y, Yu N-Y, Fang W-D, Tan Q-G, Ji R, Yang L-Y, Wei S, Zhang X-W, Miao A-J (2021b) Photodegradation of carbon dots cause cytotoxicity. Nat Commun 12:812. https://doi.org/10.1038/s41467-021-21080-z

Lu J, Yang J, Wang J, Lim A, Wang S, Loh KP (2009) One-pot synthesis of fluorescent carbon nanoribbons, nanoparticles, and graphene by the exfoliation of graphite in ionic liquids. ACS Nano 3:2367–2375. https://doi.org/10.1021/nn900546b

Lu Q, Zhang Y, Liu S (2015) Graphene quantum dots enhanced photocatalytic activity of zinc porphyrin toward the degradation of methylene blue under visible-light irradiation. J Mater Chem A 3:8552–8558. https://doi.org/10.1039/C5TA00525F

Lv Z, Wang Y, Chen J, Wang J, Zhou Y, Han S-T (2020) Semiconductor quantum dots for memories and neuromorphic computing systems. Chem Rev 120:3941–4006. https://doi.org/10.1021/acs.chemrev.9b00730

Mahat NA, Shamsudin SA (2020) Transformation of oil palm biomass to optical carbon quantum dots by carbonisation-activation and low temperature hydrothermal processes. Diam Relat Mater 102:107660. https://doi.org/10.1016/j.diamond.2019.107660

Mahat NA, Shamsudin SA, Jullok N, Ma'Radzi, A.H., (2020) Carbon quantum dots embedded polysulfone membranes for antibacterial performance in the process of forward osmosis. Desalination 493:114618. https://doi.org/10.1016/j.desal.2020.114618

Malček M, Müllerová S, Bučinský L (2022) Theoretical study of hydrogen adsorption on the graphene quantum dots doped with various first row transition metals: switch of spin state as a way to improve H_2 adsorption. Phys. E Low-dimensional Syst. Nanostructures 139:115144. https://doi.org/10.1016/j.physe.2022.115144

Markovic ZM, Ristic BZ, Arsikin KM, Klisic DG, Harhaji-Trajkovic LM, Todorovic-Markovic BM, Kepic DP, Kravic-Stevovic TK, Jovanovic SP, Milenkovic MM, Milivojevic DD, Bumbasirevic VZ, Dramicanin MD, Trajkovic VS (2012) Graphene quantum dots as autophagy-inducing photodynamic agents. Biomaterials 33:7084–7092. https://doi.org/10.1016/j.biomaterials.2012.06.060

Masters BR (2014) Paths to Förster's resonance energy transfer (FRET) theory. Eur Phys J H 39:87–139. https://doi.org/10.1140/epjh/e2013-40007-9

Meyer DE, Li M, Ingwersen WW (2020) Analyzing economy-scale solid waste generation using the United States environmentally-extended input-output model. Resour Conserv Recycl 157:104795. https://doi.org/10.1016/j.resconrec.2020.104795

Meziani MJ, Dong X, Zhu L, Jones LP, LeCroy GE, Yang F, Wang S, Wang P, Zhao Y, Yang L, Tripp RA, Sun Y-P (2016) Visible-light-activated bactericidal functions of carbon "quantum" dots. ACS Appl Mater Interfaces 8:10761–10766. https://doi.org/10.1021/acsami.6b01765

Molaei MJ (2019) Carbon quantum dots and their biomedical and therapeutic applications: a review. RSC Adv 9:6460–6481. https://doi.org/10.1039/C8RA08088G

Moradi Alvand Z, Rajabi HR, Mirzaei A, Masoumiasl A (2019a) Ultrasonic and microwave assisted extraction as rapid and efficient techniques for plant mediated synthesis of quantum dots: green synthesis, characterization of zinc telluride and comparison study of some biological activities. New J Chem 43:15126–15138. https://doi.org/10.1039/C9NJ03144H

Moradi Alvand Z, Rajabi HR, Mirzaei A, Masoumiasl A, Sadatfaraji H (2019b) Rapid and green synthesis of cadmium telluride quantum dots with low toxicity based on a plant-mediated approach after microwave and ultrasonic assisted extraction: synthesis, characterization, biological potentials and comparison study. Mater Sci Eng C 98:535–544. https://doi.org/10.1016/j.msec.2019.01.010

Muñoz R, Santos EM, Galan-Vidal CA, Miranda JM, Lopez-Santamarina A, Rodriguez JA (2021) Ternary quantum dots in chemical analysis. synthesis and detection mechanisms. Molecules 26:2764. https://doi.org/10.3390/molecules26092764

Nair A, Haponiuk JT, Thomas S, Gopi S (2020) Natural carbon-based quantum dots and their applications in drug delivery: a review. Biomed Pharmacother 132:110834. https://doi.org/10.1016/j.biopha.2020.110834

Nasrollahzadeh M, Sajjadi M, Iravani S, Varma RS (2021) Carbon-based sustainable nanomaterials for water treatment: state-of-art and future perspectives. Chemosphere 263:128005. https://doi.org/10.1016/j.chemosphere.2020.128005

National Primary Drinking Water Regulations | US EPA [WWW Document] (n.d.) URL https://www.epa.gov/ground-water-and-drinking-water/national-primary-drinking-water-regulations#Radionuclides (accessed 1.9.22)

Ng HKM, Lim GK, Leo CP (2021) Comparison between hydrothermal and microwave-assisted synthesis of carbon dots from biowaste and chemical for heavy metal detection: a review. Microchem J 165:106116. https://doi.org/10.1016/j.microc.2021.106116

Nguyen N-A, Le T-H, Trinh V-H, Ngo Q-T, Nguyen V-T, Lee G, Choi H-S, Chen G (2021) Au/Cdot-nanohybrid electrocatalyst synthesized by rice-straw-derived carbon dots as a reducing agent for improved hydrogen evolution reactions. J Electrochem Soc 168:044509. https://doi.org/10.1149/1945-7111/abf267

Nilewski L, Mendoza K, Jalilov AS, Berka V, Wu G, Sikkema WKA, Metzger A, Ye R, Zhang R, Luong DX, Wang T, McHugh E, Derry PJ, Samuel EL, Kent TA, Tsai A-L, Tour JM (2019) Highly oxidized graphene quantum dots from coal as efficient antioxidants. ACS Appl Mater Interfaces 11:16815–16821. https://doi.org/10.1021/acsami.9b01082

Pandiyan S, Arumugam L, Srirengan SP, Pitchan R, Sevugan P, Kannan K, Pitchan G, Hegde TA, Gandhirajan V (2020) Biocompatible carbon quantum dots derived from sugarcane industrial wastes for effective nonlinear optical behavior and antimicrobial activity applications. ACS Omega 5:30363–30372. https://doi.org/10.1021/acsomega.0c03290

Park SJ, Park JY, Chung JW, Yang HK, Moon BK, Yi SS (2020) Color tunable carbon quantum dots from wasted paper by different solvents for anti-counterfeiting and fluorescent flexible film. Chem Eng J 383:123200. https://doi.org/10.1016/j.cej.2019.123200

Pooja D, Singh L, Thakur A, Kumar P (2019) Green synthesis of glowing carbon dots from Carica papaya waste pulp and their application as a label-freechemo probe for chromium detection in water. Sensors Actuators B Chem 283:363–372. https://doi.org/10.1016/j.snb.2018.12.027

Pramanik S, Chatterjee S, Suresh Kumar G, Sujatha Devi P (2018) Egg-shell derived carbon dots for base pair selective DNA binding and recognition. Phys Chem Chem Phys 20:20476–20488. https://doi.org/10.1039/C8CP02872A

Prasannan A, Imae T (2013) One-pot synthesis of fluorescent carbon dots from orange waste peels. Ind Eng Chem Res 52:15673–15678. https://doi.org/10.1021/ie402421s

Qureshi WA, Vivekanandan B, Jayaprasath JA, Ali D, Alarifi S, Deshmukh K (2021) Antimicrobial activity and characterization of pomegranate peel-based carbon dots. J Nanomater 2021:1–6. https://doi.org/10.1155/2021/9096838

Raber L (1998) Chloroform is safe at levels found in tap water, says EPA. Chem Eng News Arch 76:28. https://doi.org/10.1021/cen-v076n023.p028

Rahbar M, Mehrzad M, Behpour M, Mohammadi-Aghdam S, Ashrafi M (2019) S, N co-doped carbon quantum dots/TiO_2 nanocomposite as highly efficient visible light photocatalyst. Nanotechnology 30:505702. https://doi.org/10.1088/1361-6528/ab40dc

Rajabi HR, Karimi F, Kazemdehdashti H, Kavoshi L (2018) Fast sonochemically-assisted synthesis of pure and doped zinc sulfide quantum dots and their applicability in organic dye removal from aqueous media. J Photochem Photobiol B Biol 181:98–105. https://doi.org/10.1016/j.jphotobiol.2018.02.016

Rajabi HR, Sajadiasl F, Karimi H, Alvand ZM (2020) Green synthesis of zinc sulfide nanophotocatalysts using aqueous extract of Ficus Johannis plant for efficient photodegradation of some pollutants. J Mater Res Technol 9:15638–15647. https://doi.org/10.1016/j.jmrt.2020.11.017

Rajamanikandan S, Biruntha M, Ramalingam G (2021) Blue emissive carbon quantum dots (CQDs) from bio-waste peels and its antioxidant activity. J Clust Sci. https://doi.org/10.1007/s10876-021-02029-0

Rani UA, Ng LY, Ng CY, Mahmoudi E (2020) A review of carbon quantum dots and their applications in wastewater treatment. Adv Colloid Interface Sci 278:102124. https://doi.org/10.1016/j.cis.2020.102124

Rasal AS, Yadav S, Yadav A, Kashale AA, Manjunatha ST, Altaee A, Chang J-Y (2021) Carbon quantum dots for energy applications: a review. ACS Appl Nano Mater 4:6515–6541. https://doi.org/10.1021/acsanm.1c01372

Ren X, Zhang F, Guo B, Gao N, Zhang X (2019) Synthesis of N-doped micropore carbon quantum dots with high quantum yield and dual-wavelength photoluminescence emission from biomass for cellular imaging. Nanomaterials 9:495. https://doi.org/10.3390/nano9040495

Reshak AH (2017) Quantum dots in photocatalytic applications: efficiently enhancing visible light photocatalytic activity by integrating CdO quantum dots as sensitizers. Phys Chem Chem Phys 19:24915–24927. https://doi.org/10.1039/C7CP05312F

Rodríguez-Padrón D, Algarra M, Tarelho LAC, Frade J, Franco A, de Miguel G, Jiménez J, Rodríguez-Castellón E, Luque R (2018) Catalyzed microwave-assisted preparation of carbon quantum dots from lignocellulosic residues. ACS Sustain Chem Eng 6:7200–7205. https://doi.org/10.1021/acssuschemeng.7b03848

Rosso C, Filippini G, Prato M (2020) Carbon dots as nano-organocatalysts for synthetic applications. ACS Catal 10:8090–8105. https://doi.org/10.1021/acscatal.0c01989

Sangam S, Gupta A, Shakeel A, Bhattacharya R, Sharma AK, Suhag D, Chakrabarti S, Garg SK, Chattopadhyay S, Basu B, Kumar V, Rajput SK, Dutta MK, Mukherjee M (2018) Sustainable synthesis of single crystalline sulphur-doped graphene quantum dots for bioimaging and beyond. Green Chem 20:4245–4259. https://doi.org/10.1039/C8GC01638K

Sasidharan S, Raj S, Sonawane, Shirish, Sonawane, Shriram, Pinjari D, Pandit AB, Saudagar P (2019) Nanomaterial synthesis: chemical and biological route and applications, in: Nanomaterials Synthesis. Elsevier, pp. 27–51. https://doi.org/10.1016/B978-0-12-815751-0.00002-X

Selenium in Drinking-water Background document for development of WHO Guidelines for Drinking-water Quality, 2011

Shaari N, Kamarudin SK, Bahru R (2021) Carbon and graphene quantum dots in fuel cell application: an overview. Int J Energy Res 45:1396–1424. https://doi.org/10.1002/er.5889

Singh A, Eftekhari E, Scott J, Kaur J, Yambem S, Leusch F, Wellings R, Gould T, Ostrikov K, Sonar P, Li Q (2020) Carbon dots derived from human hair for ppb level chloroform sensing in water. Sustain Mater Technol 25:e00159. https://doi.org/10.1016/j.susmat.2020.e00159

Skourtis SS, Liu C, Antoniou P, Virshup AM, Beratan DN (2016) Dexter energy transfer pathways. Proc Natl Acad Sci 113:8115–8120. https://doi.org/10.1073/pnas.1517189113

Solid Waste Management [WWW Document], n.d. URL https://www.worldbank.org/en/topic/urbandevelopment/brief/solid-waste-management. Accessed 1.21.22

Spreinat A, Dohmen MM, Lüttgens J, Herrmann N, Klepzig LF, Nißler R, Weber S, Mann FA, Lauth J, Kruss S (2021) Quantum defects in fluorescent carbon nanotubes for sensing and mechanistic studies. J Phys Chem C 125:18341–18351. https://doi.org/10.1021/acs.jpcc.1c05432

Stanković NK, Bodik M, Šiffalovič P, Kotlar M, Mičušik M, Špitalsky Z, Danko M, Milivojević DD, Kleinova A, Kubat P, Capakova Z, Humpoliček P, Lehocky M, Todorović Marković BM, Marković ZM (2018) Antibacterial and antibiofouling properties of light triggered fluorescent hydrophobic carbon quantum dots langmuir–blodgett thin films. ACS Sustain Chem Eng 6:4154–4163. https://doi.org/10.1021/acssuschemeng.7b04566

Su R, Wang D, Liu M, Yan J, Wang J-X, Zhan Q, Pu Y, Foster NR, Chen J-F (2018) Subgram-scale synthesis of biomass waste-derived fluorescent carbon dots in subcritical water for bioimaging, sensing, and solid-state patterning. ACS Omega 3:13211–13218. https://doi.org/10.1021/acsomega.8b01919

Surendran P, Lakshmanan A, Vinitha G, Ramalingam G, Rameshkumar P (2020) Facile preparation of high fluorescent carbon quantum dots from orange waste peels for nonlinear optical applications. Luminescence 35:196–202. https://doi.org/10.1002/bio.3713

Suryawanshi A, Biswal M, Mhamane D, Gokhale R, Patil S, Guin D, Ogale S (2014) Large scale synthesis of graphene quantum dots (GQDs) from waste biomass and their use as an efficient and selective photoluminescence on–off–on probe for Ag + ions. Nanoscale 6:11664–11670. https://doi.org/10.1039/C4NR02494J

Tabish TA, Zhang S (2016) Graphene quantum dots: syntheses, properties, and biological applications, in: comprehensive nanoscience and nanotechnology. Elsevier, pp. 171–192. https://doi.org/10.1016/B978-0-12-803581-8.04133-3

Tajik S, Dourandish Z, Zhang K, Beitollahi H, Le QV, Jang HW, Shokouhimehr M (2020) Carbon and graphene quantum dots: a review on syntheses, characterization, biological and sensing applications for neurotransmitter determination. RSC Adv 10:15406–15429. https://doi.org/10.1039/D0RA00799D

Talapin DV, Shevchenko EV (2016) Introduction: nanoparticle chemistry. Chem Rev 116:10343–10345. https://doi.org/10.1021/acs.chemrev.6b00566

Tam TV, Trung NB, Kim HR, Chung JS, Choi WM (2014) One-pot synthesis of N-doped graphene quantum dots as a fluorescent sensing platform for Fe^{3+} ions detection. Sensors Actuators B Chem 202:568–573. https://doi.org/10.1016/j.snb.2014.05.045

Tammina SK, Yang D, Koppala S, Cheng C, Yang Y (2019) Highly photoluminescent N, P doped carbon quantum dots as a fluorescent sensor for the detection of dopamine and temperature. J Photochem Photobiol B Biol 194:61–70. https://doi.org/10.1016/j.jphotobiol.2019.01.004

Tang D, Liu J, Yan X, Kang L (2016) Graphene oxide derived graphene quantum dots with different photoluminescence properties and peroxidase-like catalytic activity. RSC Adv 6:50609–50617. https://doi.org/10.1039/C5RA26279H

Tao S, Feng T, Zheng C, Zhu S, Yang B (2019) Carbonized polymer dots: a brand new perspective to recognize luminescent carbon-based nanomaterials. J Phys Chem Lett 10:5182–5188. https://doi.org/10.1021/acs.jpclett.9b01384

Tatrari G, Karakoti M, Tewari C, Pandey S, Bohra BS, Dandapat A, Sahoo NG (2021) Solid waste-derived carbon nanomaterials for supercapacitor applications: a recent overview. Mater Adv 2:1454–1484. https://doi.org/10.1039/D0MA00871K

Thulasi S, Kathiravan A, Asha Jhonsi M (2020) Fluorescent carbon dots derived from vehicle exhaust soot and sensing of tartrazine in soft drinks. ACS Omega 5:7025–7031. https://doi.org/10.1021/acsomega.0c00707

Tian P, Tang L, Teng KS, Lau SP (2018) Graphene quantum dots from chemistry to applications. Mater Today Chem 10:221–258. https://doi.org/10.1016/j.mtchem.2018.09.007

Tian L, Li Z, Wang P, Zhai X, Wang X, Li T (2021) Carbon quantum dots for advanced electrocatalysis. J Energy Chem 55:279–294. https://doi.org/10.1016/j.jechem.2020.06.057

Tripathi KM, Sonker AK, Sonkar SK, Sarkar S (2014) Pollutant soot of diesel engine exhaust transformed to carbon dots for multi-coloured imaging of E. coli and sensing cholesterol. RSC Adv 4:30100. https://doi.org/10.1039/C4RA03720K

Tyagi A, Tripathi KM, Singh N, Choudhary S, Gupta RK (2016) Green synthesis of carbon quantum dots from lemon peel waste: applications in sensing and photocatalysis. RSC Adv 6:72423–72432. https://doi.org/10.1039/C6RA10488F

Valizadeh A, Mikaeili H, Samiei M, Farkhani SM, Zarghami N, Kouhi M, Akbarzadeh A, Davaran S (2012) Quantum dots: synthesis, bioapplications, and toxicity. Nanoscale Res Lett 7:480. https://doi.org/10.1186/1556-276X-7-480

Vandarkuzhali SAA, Jeyalakshmi V, Sivaraman G, Singaravadivel S, Krishnamurthy KR, Viswanathan B (2017) Highly fluorescent carbon dots from Pseudo-stem of banana plant: applications as nanosensor and bio-imaging agents. Sensors Actuators B Chem 252:894–900. https://doi.org/10.1016/j.snb.2017.06.088

Vandarkuzhali SAA, Natarajan S, Jeyabalan S, Sivaraman G, Singaravadivel S, Muthusubramanian S, Viswanathan B (2018) Pineapple peel-derived carbon dots: applications as sensor, molecular keypad lock, and memory device. ACS Omega 3:12584–12592. https://doi.org/10.1021/acsomega.8b01146

Vatanpour V, Karatas O, Amiri S, Rajabi HR, Koyuncu I, Khataee A (2022) Different metal-doped ZnS quantum dots photocatalysts for enhancing the permeability and antifouling performances of polysulfone membranes with and without UV irradiation. Chemosphere 294:133705. https://doi.org/10.1016/j.chemosphere.2022.133705

Venkatesan S, Mariadoss AJ, Arunkumar K, Muthupandian A (2019) Fuel waste to fluorescent carbon dots and its multifarious applications. Sensors Actuators B Chem 282:972–983. https://doi.org/10.1016/j.snb.2018.11.144

Wang Q, Liu X, Zhang L, Lv Y (2012) Microwave-assisted synthesis of carbon nanodots through an eggshell membrane and their fluorescent application. Analyst 137:5392. https://doi.org/10.1039/c2an36059d

Wang D, Zhu L, Chen J-F, Dai L (2015a) Can graphene quantum dots cause DNA damage in cells? Nanoscale 7:9894–9901. https://doi.org/10.1039/C5NR01734C

Wang Y, Wu W, Wu M, Sun H, Xie H, Hu C, Wu X, Qiu J (2015b) Yellow-visual fluorescent carbon quantum dots from petroleum coke for the efficient detection of Cu^{2+} ions. New Carbon Mater 30:550–559. https://doi.org/10.1016/S1872-5805(15)60204-9

Wang L, Li W, Wu B, Li Z, Wang S, Liu Y, Pan D, Wu M (2016a) Facile synthesis of fluorescent graphene quantum dots from coffee grounds for bioimaging and sensing. Chem Eng J 300:75–82. https://doi.org/10.1016/j.cej.2016.04.123

Wang Y, Hu A (2014) Carbon quantum dots: synthesis, properties and applications. J Mater Chem C 2:6921. https://doi.org/10.1039/C4TC00988F

Wang S, Cole IS, Li Q (2016b) The toxicity of graphene quantum dots. RSC Adv 6:89867–89878. https://doi.org/10.1039/C6RA16516H

Wang Z, Fu B, Zou S, Duan B, Chang C, Yang B, Zhou X, Zhang L (2016c) Facile construction of carbon dots via acid catalytic hydrothermal method and their application for target imaging of cancer cells. Nano Res 9:214–223. https://doi.org/10.1007/s12274-016-0992-2

Wang Z, Yu J, Zhang X, Li N, Liu B, Li Y, Wang Y, Wang W, Li Y, Zhang L, Dissanayake S, Suib SL, Sun L (2016d) Large-scale and controllable synthesis of graphene quantum dots from rice husk biomass: a comprehensive utilization strategy. ACS Appl Mater Interfaces 8:1434–1439. https://doi.org/10.1021/acsami.5b10660

Wang R, Xia G, Zhong W, Chen L, Chen L, Wang Y, Min Y, Li K (2019a) Direct transformation of lignin into fluorescence-switchable graphene quantum dots and their application in ultrasensitive profiling of a physiological oxidant. Green Chem 21:3343–3352. https://doi.org/10.1039/C9GC01012B

Wang Z-X, Gao Y-F, Jin X, Yu X-H, Tao X, Kong F-Y, Fan D-H, Wang W (2019b) Excitation-independent emission carbon nanoribbon polymer as a ratiometric photoluminescent probe for highly selective and sensitive detection of quercetin. Analyst 144:2256–2263. https://doi.org/10.1039/C9AN00094A

Wang C, Shi H, Yang M, Yan Y, Liu E, Ji Z, Fan J (2020) Facile synthesis of novel carbon quantum dots from biomass waste for highly sensitive detection of iron ions. Mater Res Bull 124:110730. https://doi.org/10.1016/j.materresbull.2019.110730

Wang X, Ma Y, Wu Q, Wang Z, Tao Y, Zhao Y, Wang B, Cao J, Wang H, Gu X, Huang H, Li S, Wang X, Hu F, Shao M, Liao L, Sham T, Liu Y, Kang Z (2021) Ultra-bright and stable pure blue light-emitting diode from O, N Co-doped carbon dots. Laser Photon Rev 15:2000412. https://doi.org/10.1002/lpor.202000412

Wareing TC, Gentile P, Phan AN (2021) Biomass-based carbon dots: current development and future perspectives. ACS Nano 15:15471–15501. https://doi.org/10.1021/acsnano.1c03886

Wei J, Zang Z, Zhang Y, Wang M, Du J, Tang X (2017) Enhanced performance of light-controlled conductive switching in hybrid cuprous oxide/reduced graphene oxide (Cu_2O/rGO) nanocomposites. Opt Lett 42:911. https://doi.org/10.1364/OL.42.000911

Welsher K, Liu Z, Sherlock SP, Robinson JT, Chen Z, Daranciang D, Dai H (2009) A route to brightly fluorescent carbon nanotubes for near-infrared imaging in mice. Nat Nanotechnol 4:773–780. https://doi.org/10.1038/nnano.2009.294

Wu P, Li W, Wu Q, Liu Y, Liu S (2017) Hydrothermal synthesis of nitrogen-doped carbon quantum dots from microcrystalline cellulose for the detection of Fe^{3+} ions in an acidic environment. RSC Adv 7:44144–44153. https://doi.org/10.1039/C7RA08400E

Xu X, Ray R, Gu Y, Ploehn HJ, Gearheart L, Raker K, Scrivens WA (2004) Electrophoretic analysis and purification of fluorescent single-walled carbon nanotube fragments. J Am Chem Soc 126:12736–12737. https://doi.org/10.1021/ja040082h

Xu Q, Gong Y, Zhang Z, Miao Y, Li D, Yan G (2019) Preparation of graphene oxide quantum dots from waste toner, and their application to a fluorometric DNA hybridization assay. Microchim Acta 186:483. https://doi.org/10.1007/s00604-019-3539-x

Xu D, Lin Q, Chang H (2020) Recent advances and sensing applications of carbon dots. Small Methods 4:1900387. https://doi.org/10.1002/smtd.201900387

Xu-Cheng F, Xuan-Hua L, Jin J-Z, Zhang J, Wei G (2018) Facile synthesis of bagasse waste derived carbon dots for trace mercury detection. Mater Res Express 5:065044. https://doi.org/10.1088/2053-1591/aaccb7

Xue M, Zhan Z, Zou M, Zhang L, Zhao S (2016) Green synthesis of stable and biocompatible fluorescent carbon dots from peanut shells for multicolor living cell imaging. New J Chem 40:1698–1703. https://doi.org/10.1039/C5NJ02181B

Yan C, Hu X, Guan P, Hou T, Chen P, Wan D, Zhang X, Wang J, Wang C (2020) Highly biocompatible graphene quantum dots: green synthesis, toxicity comparison and fluorescence imaging. J Mater Sci 55:1198–1215. https://doi.org/10.1007/s10853-019-04079-2

Yang HB, Miao J, Hung S-F, Huo F, Chen HM, Liu B (2014) Stable quantum dot photoelectrolysis cell for unassisted visible light solar water splitting. ACS Nano 8:10403–10413. https://doi.org/10.1021/nn503751s

Yang H, Zhou B, Zhang Y, Liu H, Liu Y, He Y, Xia S (2021) Valorization of expired passion fruit shell by hydrothermal conversion into carbon quantum dot: physical and optical properties. Waste and Biomass Valorization 12:2109–2117. https://doi.org/10.1007/s12649-020-01132-z

Yao Y-Y, Gedda G, Girma WM, Yen C-L, Ling Y-C, Chang J-Y (2017) Magnetofluorescent carbon dots derived from crab shell for targeted dual-modality bioimaging and drug delivery. ACS Appl Mater Interfaces 9:13887–13899. https://doi.org/10.1021/acsami.7b01599

Ye R, Xiang C, Lin J, Peng Z, Huang K, Yan Z, Cook NP, Samuel ELG, Hwang C-C, Ruan G, Ceriotti G, Raji A-RO, Martí AA, Tour JM (2013) Coal as an abundant source of graphene quantum dots. Nat Commun 4:2943. https://doi.org/10.1038/ncomms3943

Ye Q, Yan F, Luo Y, Wang Y, Zhou X, Chen L (2017) Formation of N, S-codoped fluorescent carbon dots from biomass and their application for the selective detection of mercury and iron ion. Spectrochim. Acta Part A Mol Biomol Spectrosc 173:854–862. https://doi.org/10.1016/j.saa.2016.10.039

Ye Z, Zhang Y, Li G, Li B (2020) Fluorescent determination of mercury(II) by green carbon quantum dots synthesized from eggshell membrane. Anal Lett 53:2841–2853. https://doi.org/10.1080/00032719.2020.1759618

Yoo D, Park Y, Cheon B, Park M-H (2019) Carbon dots as an effective fluorescent sensing platform for metal ion detection. Nanoscale Res Lett 14:272. https://doi.org/10.1186/s11671-019-3088-6

Youh M-J, Jiang M-Y, Chung M-C, Tai H-C, Li Y-Y (2020) Formation of graphene quantum dots by ball-milling technique using carbon nanocapsules and sodium carbonate. Inorg Chem Commun 119:108061. https://doi.org/10.1016/j.inoche.2020.108061

Younis MR, He G, Lin J, Huang P (2020) Recent advances on graphene quantum dots for bioimaging applications. Front Chem 8:424. https://doi.org/10.3389/fchem.2020.00424

Yu C, Jiang X, Qin D, Mo G, Zheng X, Deng B (2019) Facile syntheses of s, n-codoped carbon quantum dots and their applications to a novel off–on nanoprobe for detection of 6-thioguanine and its bioimaging. ACS Sustain Chem Eng 7:16112–16120. https://doi.org/10.1021/acssuschemeng.9b02886

Yuan M, Zhong R, Gao H, Li W, Yun X, Liu J, Zhao X, Zhao G, Zhang F (2015) One-step, green, and economic synthesis of water-soluble photoluminescent carbon dots by hydrothermal treatment of wheat straw, and their bio-applications in labeling, imaging, and sensing. Appl Surf Sci 355:1136–1144. https://doi.org/10.1016/j.apsusc.2015.07.095

Yun X, Li J, Chen X, Chen H, Xiao L, Xiang K, Chen W, Liao H, Zhu Y (2019) Porous Fe 2 O 3 modified by nitrogen-doped carbon quantum dots/reduced graphene oxide composite aerogel as a high-capacity and high-rate anode material for alkaline aqueous batteries. ACS Appl Mater Interfaces 11:36970–36984. https://doi.org/10.1021/acsami.9b12827

Zammataro A, Sfrazzetto GT (2019) Carbon dots as catalysts: a new class of nanozymes. Curr Organocatalysis 7:3–6. https://doi.org/10.2174/2213337206666190702165008

Zang Z, Zeng X, Wang M, Hu W, Liu C, Tang X (2017) Tunable photoluminescence of water-soluble AgInZnS–graphene oxide (GO) nanocomposites and their application in-vivo bioimaging. Sensors Actuators B Chem 252:1179–1186. https://doi.org/10.1016/j.snb.2017.07.144

Zdrazil L, Zahradnicek R, Mohan R, Sedlacek P, Nejdl L, Schmiedova V, Pospisil J, Horak M, Weiter M, Zmeskal O, Hubalek J (2018) Preparation of graphene quantum dots through liquid phase exfoliation method. J Lumin 204:203–208. https://doi.org/10.1016/j.jlumin.2018.08.017

Zhang B, Liu Y, Ren M, Li W, Zhang X, Vajtai R, Ajayan PM, Tour JM, Wang L (2019) Sustainable synthesis of bright green fluorescent nitrogen-doped carbon quantum dots from alkali lignin. Chemsuschem 12:4202–4210. https://doi.org/10.1002/cssc.201901693

Zhao S, Rondin L, Delport G, Voisin C, Beser U, Hu Y, Feng X, Müllen K, Narita A, Campidelli S, Lauret JS (2017) Fluorescence from graphene nanoribbons of well-defined structure. Carbon n y 119:235–240. https://doi.org/10.1016/j.carbon.2017.04.043

Zhao C, Song X, Liu Y, Fu Y, Ye L, Wang N, Wang F, Li L, Mohammadniaei M, Zhang M, Zhang Q, Liu J (2020) Synthesis of graphene quantum dots and their applications in drug delivery. J Nanobiotechnology 18:142. https://doi.org/10.1186/s12951-020-00698-z

Zhu J, Zhu F, Yue X, Chen P, Sun Y, Zhang L, Mu D, Ke F (2019) Waste utilization of synthetic carbon quantum dots based on tea and peanut shell. J Nanomater 2019:1–7. https://doi.org/10.1155/2019/7965756